8-2019

Evaluating the therapeutic efficacy of Grb2 inhibition in ovarian malignancies

Olivia Lara

EVALUATING THE THERAPEUTIC EFFICACY OF GRB2 INHIBITION IN OVARIAN MALIGNANCIES

By

Olivia D. Lara, M.D.

APPROVED:

_____
Anil K. Sood, M.D.
Advisory Professor

_____
Funda Meric-Bernstam, M.D.

_____
Cristian Rodriguez-Aguayo, Ph.D.

_____
Wei Hu, M.D., Ph.D.

_____
Vahid Afshar-Kharghan, M.D.

APPROVED:

_____
Dean, The University of Texas
MD Anderson Cancer Center UTHealth Graduate School of Biomedical Sciences

EVALUATING THE THERAPEUTIC EFFICACY OF GRB2 INHIBITION IN OVARIAN MALIGNANCIES

A

Thesis

Presented to the Faculty of

The University of Texas

MD Anderson Cancer Center

UT Health Graduate School of Biomedical Sciences

In Partial Fulfillment

Of the Requirements

For the Degree of

MASTER OF SCIENCE

by

Olivia D. Lara, M.D.
Houston, Texas

August, 2019

Acknowledgments

I would like to thank my thesis mentor, Dr. Anil Sood. His mentorship has been critical in my success. He has made my time in the lab extremely rewarding, and has not only taught me to be a thoughtful scientist, but also impacted how I will practice medicine. A special thank you to Cristian Rodriguez-Aguayo for his guidance, patience and encouragement over the past two years.

Thank you to all the members of the Sood and Lopez lab for all their ideas, support, and teaching they have provided. Thank you to Emine Bayraktar for showing me how to do my first western blot, and for her patience in teaching me various lab techniques. Thank you also to Mangala, and Shaolin for their ideas and support to help move this project forward.

Finally a thank you to all my committee members for their input and feedback that have contributed to the success of this work.

EVALUATING THE THERAPEUTIC EFFICACY OF GRB2 INHIBITION IN OVARIAN MALIGNANCIES

Olivia D. Lara, M.D.

Advisory Professor: Anil K. Sood, M.D.

Abstract

Purpose: Adaptor proteins such as growth factor receptor-bound protein-2 (Grb2) play important roles in cancer cell signaling. In the present study, we examined the biological effects of liposomal antisense oligodeoxynucleotide that blocks Grb2 expression (L-Grb2) in ovarian cancer models.

Experimental Design: Murine orthotopic models of ovarian cancer (OVCAR5 and SKOV3ip1) were used to study the biological effects of L-Grb2 on tumor growth. *In vitro* experiments (cell viability assay, Western blot analysis, siRNA transfection, and reverse phase protein array) were carried out to elucidate the mechanism and potential predictors of tumor response to L-Grb2.

Results: Treatment with L-Grb2 decreased tumor growth and metastasis in orthotopic models of ovarian cancer (OVCAR5, SKOV3ip1) by reducing angiogenesis and increasing apoptosis at a dose of 15 mg/kg with no effect on mouse body weight. Treatment with L-Grb2 and paclitaxel led to the greatest decrease in tumor weight (mean± SEM, 0.17 g ± 0.10 g) compared with that in control mice (0.99 g ± 0.35 g). We also observed a reduction in tumor burden after treatment with L-Grb2 and the anti-VEGF antibody B-20 (86% decrease in tumor weight compared with that in controls). Ovarian cancer cells with ErbB2 amplification (OVCAR8 and SKOV3ip1) were the most sensitive

to Grb2 downregulation. Reverse phase protein array analysis identified significant dysregulation of metabolites (LDHA, GAPDH, and TCA intermediates) in ovarian cancer cells after Grb2 downregulation.

Conclusions: L-Grb2 has therapeutic efficacy in preclinical models of ovarian cancer. These findings support the clinical development of L-Grb2 for treatment of cancer.

Table of Contents

List of Figures

List of Tables

1. Background and Introduction

1.1 Ovarian cancer statistics and standard of care

Ovarian cancer ranks among the most lethal types of malignancies of the female reproductive system and comprises a molecularly diverse range of tumors.[9] In 2019, there will be approximately 22,000 new cases ovarian cancer diagnosed and 14,000 ovarian cancer death in the United States. [1] A woman's risk of ovarian cancer during her lifetime is about 1 in 70, while her lifetime chance of dying from ovarian cancer is about 1 in 100.[2] Histologically, ovarian tumors range from epithelial, sex cord-stromal and germ cell origin. However the majority of ovarian cancers are of epithelial origin, of which high grade serous carcinoma is the most common histologic subtype making up >70% of ovarian carcinomas.[3] The additional four subtypes of epithelial cancers occur at lower frequency and have more favorable prognosis.[4] These include endometrioid, clear cell, mucinous and low-grade serous carcinomas which collectively account for approximately 25% of the remaining ovarian carcinomas.[3] Each histologic subtype of ovarian cancer represents clinically and molecularly different tumors with unique origin precursors. [5,6] For example high grade serous carcinoma is thought to originate from serous tubal intraepithelial carcinoma (STIC), an early pre-invasive lesion in the fallopian tube,[7] while endometrioid and clear cell carcinomas may develop from endometriosis.[8]

In addition to the cellular and molecular differences between histological subtypes, ovarian cancer often presents at a late stage making treatment challenging. Early ovarian cancer often has no obvious symptoms, with most women reporting vague, nonspecific symptoms. The most common sign of ovarian cancer is abdominal swelling, which occurs

at the late stages of cancer development. Only 20% of patients with ovarian cancer are diagnosed at an early stage, for which 5 year survival reaches 90%.[9] However the majority of patients present with higher stage disease for which 5 year overall survival is a dismal 29%. (**Table 1**).

Table 1. Ovarian Cancer stage and five year overall survival [9,10]

FIGO Stage	Criteria	5-year survival
IA	Tumor limited to one ovary or fallopian tube	89.6
IB	Tumor limited to both ovaries or fallopian tubes	86.1
IC	Tumor limited to one or both ovaries or fallopian tubes with surgical spill/capsule rupture or malignant ascites	83.4
IIA	Extension and/or implants on the uterus and/or fallopian tubes and/or ovaries	70.7
IIB	Extension to and/or implants on other pelvic tissues	65.5
IIIA	Microscopic extrapelvic peritoneal involvement +/- retroperitoneal lymph nodes	46.7
IIIB	Macroscopic peritoneal metastasis 2cm or less	41.5
IIIC	Macroscopic peritoneal metastasis more than 2cm	32.5
IV	Distant metastasis including pleural effusion with positive cytology	18.6

Surgical staging and cytoreduction followed by adjuvant chemotherapy is the management approach used for most patients with ovarian carcinoma.[11] Surgical staging entails total hysterectomy with bilateral salpingo-oophorectomy, pelvic and paraaortic lymph node dissection, omentectomy, and assessment of abdominal cavity with biopsies.[12] Cytoreductive surgery is performed with the goal to remove all gross residual disease.[13] The ability to remove macroscopic disease with cytoreductive surgery correlates with improvements in survival.[14] In patients with early stage ovarian carcinoma surgery is followed by adjuvant taxane and platinum based chemotherapy regimens. Despite initial response to therapy, the majority of patients will relapse and require retreatment. In the relapse setting there are several treatment options available, but the ideal treatment option is not known. These include cytotoxic drugs, doxorubicin, gemcitabine, and topotecan, as well as new agents such as bevacizumab and poly-ADP ribose polymerase (PARP) inhibitors. Improvements in surgical technique and the development of targeted therapies have led to a decreasing incidence rate in ovarian carcinoma,[4] however the overall cure rate remains 30%.[15] Given the clinical and genetic heterogeneity of ovarian cancer, prolonging survival might be achieved by targeting cellular and molecular mechanisms important to tumor pathogenesis.

1.2 Molecular Alterations in Ovarian Cancer

While changes in chemotherapy regimens and the addition of bevacizumab and PARP inhibitor therapies have considerably improved outcomes, they appear to have reached their therapeutic ceiling. Additionally PARP inhibitors have primarily demonstrated efficacy in recurrent ovarian cancer patients with germline BRCA1/2 mutations, or

deficiencies in homologous recombination.[16] Unfortunately ovarian cancer lags behind a number of solid malignancies in the number of therapies available.[17] The identification of potential molecular targets and novel therapies are desperately needed to prolong survival especially in high grade ovarian carcinoma. In order to develop such therapies, we must better understand genomic abnormalities that influence pathology, and constitute therapeutic targets.

Currently we know mutation and loss of TP53 function, and copy number alterations are the most frequent observed abnormality in high grade serous ovarian cancers. [18,19] While the centrality of TP53 to ovarian cancers has been established, clinically restoring p53 function has not proven to be of clinical benefit.[20] Other somatic mutations found to be significantly altered in ovarian carcinoma include BRCA1, BRCA2, RB1, CDK12, and NF1.[19] The high prevalence of BRCA pathway alterations in ovarian carcinoma have resulted in the use of PARP inhibitors with corresponding good responses. An additional challenge is the heterogeneity within histologic subtypes of ovarian cancer (**Table 2**).[15]

Table 2. Molecular Features of epithelial ovarian tumors

Histology	**Mutation**
Low-grade serous carcinoma	KRAS and/or BRAF
Low-grade endometrioid carcinoma	CTNNB1, PTEN, PIK3CA, microsatellite instability
Mucinous carcinoma	KRAS, TP53
Clear cell carcinoma	PTEN, PIK3CA
High-grade serous carcinoma	TP53 (80%), BRCA1
High-grade endometrioid carcinoma	TP53, BRCA1, PIK3CA

Published studies have integrated genomic data to analyze the most frequently disturbed cancer-associated pathways according to mutations, changes in gene expression and copy number changes. Mutations in RAS/RAF/MAPK pathway are found in more than 50% of low grade serous carcinomas while PI3K/AKT/mTOR signaling pathway is altered in 70% of high grade serous carcinomas. [21-24] These alterations suggest that targeting components of either pathway may represent a useful strategy in ovarian cancer.

1.3 Targeting Therapies in Development

MAPK and PI3K/AKT/mTOR cell signaling pathways play important roles in cell growth, proliferation, and survival. Mutations of these pathways is frequently implicated in a number of solid tumors, and the development of inhibitors has already been undertaken

and can potentially be translated to ovarian carcinoma.[25] For instance, up to 35% of patients with low grade serous carcinoma will harbor V600E BRAF mutations, usually confined to early stage disease.[26] Administration of debrafenib and trametinib combination therapy, BRAF and MEK1/2 inhibitor therapy, yielded positive results in a patient with low-grade serous carcinoma. [27] RO5126766 is a first-in-class dual MEK/RAF inhibitor currently in early development for advanced solid tumors. RO5126766 was assessed in a phase 1 study of solid tumors including ovarian cancer (n=6). A modest reduction in tumor size was seen in 40% of patients across tumor types.[28] Simultaneous inhibition of both pathways with MEK1/2 inhibitor, pimasertib, and dual PI3K/mTOR inhibitor, SAR245409, suggested signs of clinical activity in three patients with low-grade ovarian carcinoma in a phase 1 clinical trial. [29]

Additional therapeutics in development include inhibitors of EGFR and ErbB2 (HER2) which are required for activation of MAPK and PI3K/AKT pathways. Gefitinib (EGFR inhibitor) yielded modest efficacy in advance solid tumors including ovarian carcinoma.[30] The addition of EGFR inhibitor, erlotinib, to paclitaxel and carboplatin also appeared to be favorable to paclitaxel and carboplatin only in patients with resected disease. [31] ErbB2 is overexpressed in 11% of ovarian cancers. Trastuzumab, anti-HER2 antibody, yielded an overall response of 7.3% with one complete and two partial responses in patients with recurrent or refractory ovarian carcinoma. [32]

While current therapies are promising for ovarian cancer patients, a closer look at these cancer signaling pathways may reveal additional therapeutic targets. Taking a closer

look at MAPK and PI3K/AKT/mTOR pathways common signaling activation through receptor tyrosine kinases (RTKs) and growth factor receptors is noted (**Figure 1**). Upon activation, either by ligand binding or protein overexpression, dimerization and stabilization of RTKs occurs, resulting in stimulation of tyrosine kinase activates and auto-phosphorylation on tyrosine residues. [33,34] Phosphotyrosine residues are then used as docking sites for various proteins. One such protein is growth factor receptor-bound protein-2 (Grb2). Adaptor proteins such as Grb2 are essential for signal propagation after receptor tyrosine kinase activation.[35] Grb2 is a 25kDa adaptor protein which uses its SH2 domain to bind to phosphotyrosine residues found in RTKs (EGFR, ErbB2, VEGF) and its SH3 domains to bind to proline-rich motifs, such as those found in guanine nucleotide exchange factor Son of Sevenless (SOS).[36-39] SOS activation leads to activation of RAS ultimately increasing RAF, MEK and ERK activity.[40,41] Besides guanine nucleotide exchange factors, Grb2 has been demonstrated to use its SH3 domain to bind to proline-rich proteins such as phosphatidylinositol 3-kinase (PI3K). PI3K activity can also occur due to activating mutations of RAS showing the crosstalk that exists between pathways. Therefore targeting one pathway may result in activation of another as a compensatory mechanism. Because of Grb2's central location, and crucial involvement in transducing the signals of oncogenic tyrosine kinases to downstream mediators it is an attractive therapeutic target.

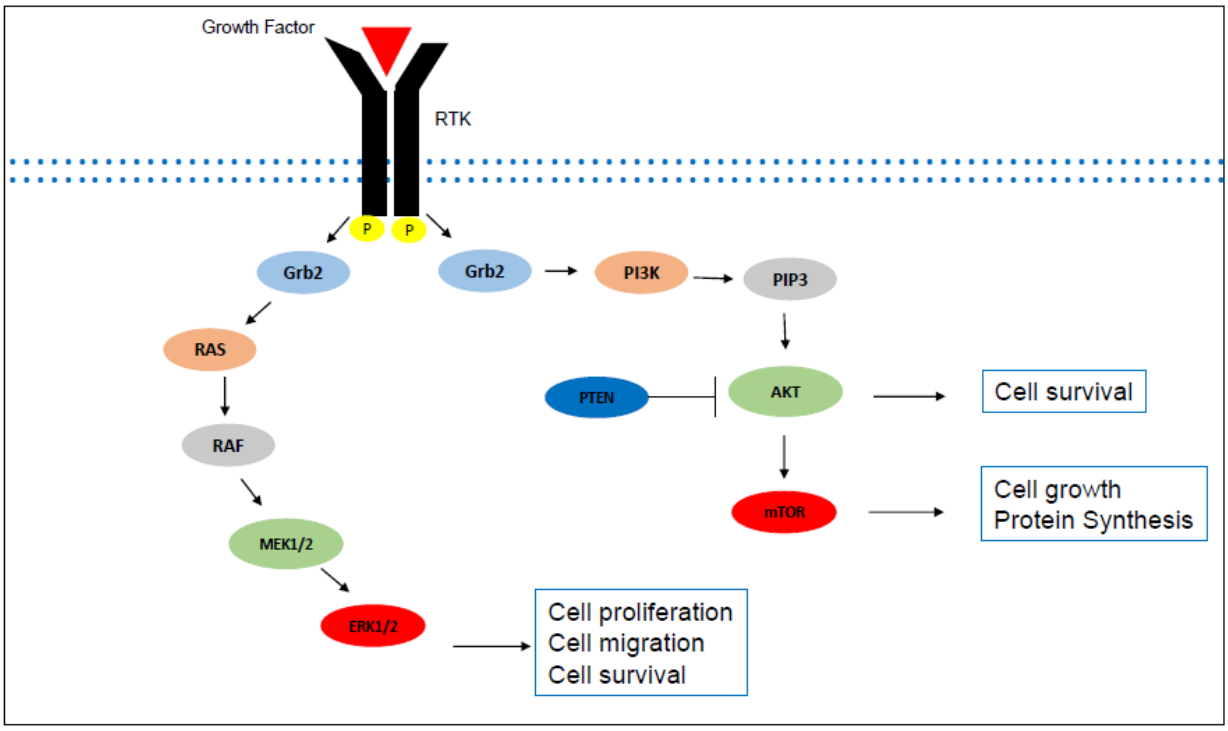

Figure 1. Overview of RTK signaling

1.4 Nucleic-Acid based therapeutics

Key adaptor proteins, such as Grb2, have previously thought to be undruggable molecular targets. Actionable targets have often been proteins with an enzymatically active site to which a small molecule could bind, however the ability to target previously undruggable targets is evolving. Small molecule inhibitors rely on intracellular targets, or antibodies to inhibit growth factors, cell surface receptors or cytokines[42,43]. More recently the use of nucleic acid based therapeutics, which allows for the regulation of gene expression, has been employed to inhibit elusive targets [44,45]. Nucleic-acid based therapeutics is a process in which RNA molecules or antisense oligonucleotides (ASOs) inhibit gene expression or translation by neutralizing targeted mRNA molecules.[46,47] A double-stranded RNA molecule silences gene expression by inducing degradation of a

complimentary mRNA. Small interfering RNAs (siRNA), and antisense oligonucleotides (ASO) are the most commonly used methods of gene silencing (**Figure 2**).

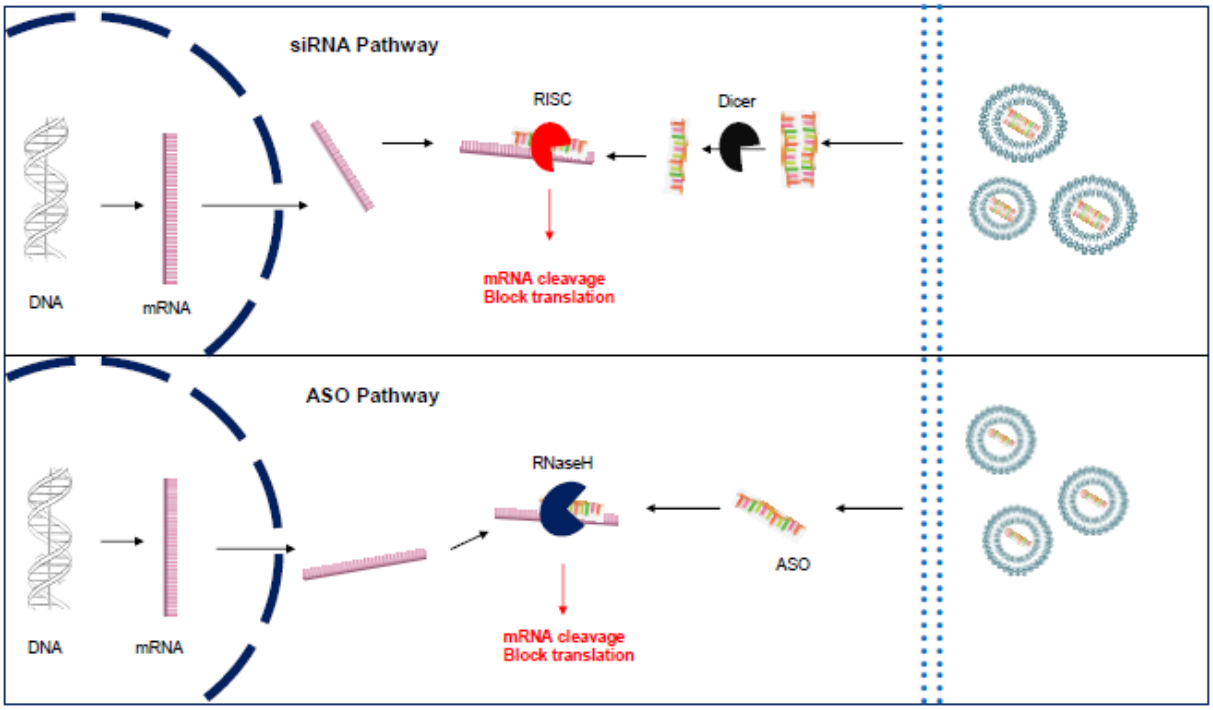

Figure 2. Methods of nucleic-acid based interference

SiRNA interact with RNA-induced silencing complex to block and neutralize the target mRNA.[48,49] Larger siRNAs require processing by ribonuclease III-like DICER enzyme. DNA/RNA-like ASOs bind to RNA through complementary base pair interactions. After crossing the cell membrane ASOs target mRNA direction, in the nucleus or cytosol, thus blocking and neutralizing the targeted mRNAs. Both siRNA and ASOs provide specific and efficient knockdown of gene expression. Comparisons between siRNA and ASO in *in vitro* assays have shown that siRNA leads to quicker and more durable gene knockdown compared to ASO.[50] This may translate to lower doses with less frequency

in patients. Both siRNA and ASOs have been associated with nonspecific toxicity at high doses *in vivo*.[51] However, the antisense approach is a mature method with proven efficacy in human trials. SiRNA remains a novel technology with increase costs, for which new problems may be encountered.

RNA is rapidly degraded in circulation due to RNAases and requires formulations into nanoparticles to carry them to their target tissues (**Figure 3**).[52,53] Liposomes have been widely studied and utilized for targeted drug delivery.[52] The ability of liposomes to interact with cells and aid in drug delivery strongly depends on the density and charge on the liposome surface. Both cationic (positively charged) and anionic (negatively charged) liposomes have shown encouraging results in *in vitro* and *in vivo* experiments. However due to their electrostatic properties they are can cause a number of side effects including rapid uptake by reticuloendothelial system (RES), leading to cytokine storm and acute pulmonary toxicity.[54-56] Because of their positive charge, cationic liposomes are less likely to be taken up by cells as well. Neutral liposomes (no surface charge) produce less side effects, but lack stability leading to increased aggregation.[57,58] Overall liposomes provide a valid method of delivery of synthetic siRNA and ASOs.

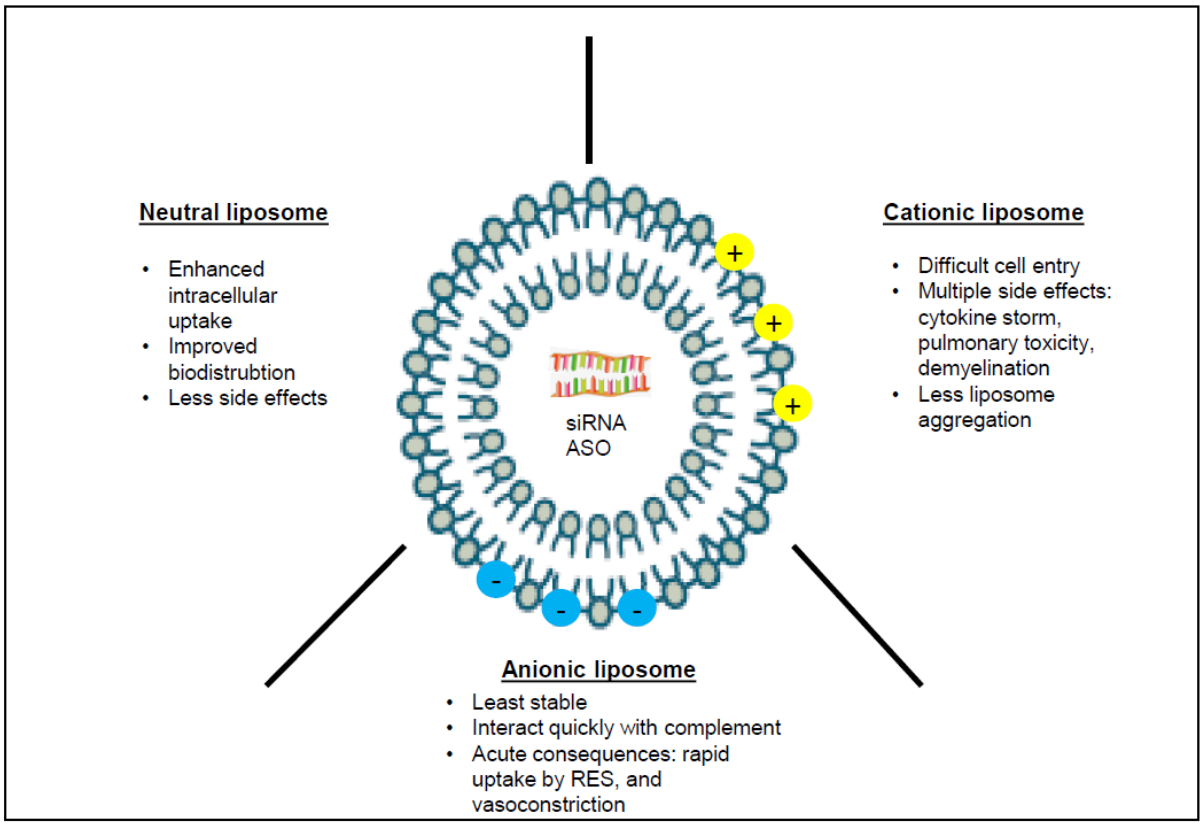

Figure 3. Liposome delivery system

Here we focused on testing the anticancer effects of ASO that blocks Grb2 protein expression (L-Grb2) incorporated into a neutral liposome. The high prevalence of molecular alterations in the MAPK and PI3K/AKT/mTOR pathways in ovarian carcinoma, combined with this novel therapeutic system represents an important therapeutic opportunity.

2. Hypothesis and Specific Aims

2.1 Hypothesis: The central goal of this project was to elucidate the role of Grb2 in ovarian malignancies. Specifically we evaluated the efficacy of Grb2 inhibition in ovarian tumor models and *in vitro* experiments to establish rationale for the use of L-Grb2 as an ovarian cancer therapeutic. We hypothesized Grb2 inhibition will reduce tumor growth by interfering with receptor tyrosine kinase signaling (Ras/Raf/MAPK and PI3K/AKT/mTOR pathways) critical to carcinogenesis.

2.2 Specific Aim 1: To determine the biological efficacy of L-Grb2 in ovarian tumor models and *in vitro* assays

2.3 Specific Aim 2: To determine the mechanisms responsible for biological effects of Grb2 downregulation and identify potential predictors of response to L-Grb2 therapy.

3. Materials and Methods

3.1 Cell line maintenance and siRNA transfection

The ovarian cancer cell lines OVCAR8, HeyA8, A2780ip1, and SKOV3ip1 were maintained in RPMI 1640 medium supplemented with 10% FBS and 0.1% gentamicin sulfate (Gemini Bioproducts). OVCAR5 ovarian cells and KLE uterine cells were maintained in Dulbecco's modified Eagle's medium with 10% FBS and 0.1% gentamicin sulfate. RF-24 endothelial cells were maintained in Dulbecco's modified Eagle's medium (MEM) supplemented with pyruvate, amino acids, and penicillin/streptomycin. Uterine cancer cell lines MFE319, Ishikawa were maintained in MEM supplemented with 10% FBS and 0.1% gentamicin sulfate Hec1a uterine cells were maintained in MCoy's 5A supplemented with 10% FBS and 0.1% gentamicin sulfate. All of these cells were cultured at 37°C using a 5% CO_2 incubator. Cell line authentication was performed by the Characterized Cell Line Core at The University of Texas MD Anderson Cancer Center. Mycoplasma testing of the cells was performed using an ATCC Universal Mycoplasma Detection Kit. All *in vitro* experiments were conducted with 80% confluent cultures and fewer than 20 passages. Ovarian cancer cells were transfected with Grb2 siRNA or control siRNA. All siRNA sequences were purchased from Sigma-Aldrich (SASI_Hs01_00129586). Cells were seeded in six-well plates at a density that yielded 50-60% confluence after 24 hours of platting (100,000 to 150,000 cells/well). The next day, 1.3 μL (100 nm) of siGrb2 sequences were mixed at a 1:3 ratio with Lipofectamine 2000 (lot #1774775; Invitrogen) prepared in serum-free medium for 20 minutes. The transfection complex was added to cells with serum-free medium. Cells were incubated

with the siRNA/Lipofectamine 2000 complex for 4 hours in a 37°C, 5% CO_2 incubator and refreshed with complete medium after 4 hours. Cells were then harvested for Western blot analysis to verify Grb2 knockdown. For transfection in 96-well plates, cells were plated at a density of 5,000-7,000 cells per well in technical replicates in six wells per siRNA sequence. The next day, cells were transfected with 0.21 μL of siRNA in serum-free media and incubated for 4 hours in a tissue culture incubator as described above. Cells were then re-fed with complete media and subjected to alamarBlue viability assays.

3.2 Cell viability assays

Cell viability assays were performed by testing cells' ability to reduce alamarBlue (Bio-Rad). Ovarian cancer cell lines were seeded in a 96-well plate and transfected the next day with increasing concentrations of siControl or siGrb2. After 72 hours, cells were incubated with 0.10% alamarBlue for 4 hours at 37°C. The absorbance at 540 nm was then recorded.

3.3 Immunoblotting

After siRNA transfection, cells were harvested and lysed with RIPA buffer (1% Triton X-100, 25 mM Tris, 150 mM NaCl, 0.1% SDS, 0.5% sodium deoxycholate) supplemented with fresh protease and phosphatase inhibitors (TC260670 and TJ272575; Thermo Fisher Scientific). Protein quantification was performed using a BCA Protein Assay Kit (#23235; Thermo Fisher Scientific) following the manufacturer's protocol. Thirty micrograms of cell lysates was loaded onto SDS-PAGE gels. After

separation, proteins were transferred to nitrocellulose membranes and blocked with 5% nonfat dry milk (#AB10109-0100; AmericanBio) in TBS-T (0.1% Tween-20) for 1 hour at room temperature. After blocking, indicated antibodies diluted in 5% milk in TBS-T were placed on membrane overnight at 4°C. The next day, the membranes were washed three times with TBS-T for 10 minutes with light agitation. Afterward, a species-specific secondary antibody was placed on membrane for 2 hours at room temperature. The membranes were then washed three times in TBS-T and finally developed using Western Lightning Plus-ECL (#NEL105001EA; PerkinElmer) on X-ray film (#F-BX57; Phoenix Research Products). For re-probing of Western blots, membranes were stripped using Restore PLUS Western Blot Stripping Buffer (#46430; Thermo Fisher Scientific), re-blocked with 5% milk in TBS-T, and incubated with a primary antibody. The antibody dilutions were as follows: anti-Grb2, 1:1000 (#3972; Cell Signaling Technology); anti-ErbB2, 1:100 (2242S; Cell Signaling Technology), anti-vinculin, 1:2000 (V9131, lot #118M4777V; Sigma), anti-β-actin, 1:2000 (127M4866V; Sigma), anti-GAPDH, 1:1000 (5174, Cell Signaling Technology), anti-LDHA, 1:1000 (3582, Cell Signaling Technology), anti-c-MYC, 1:1000 (5605, Cell Signaling Technology) and anti-SOD2 (13141, Cell Signaling Technology).

3.4 Murine orthotopic models of ovarian carcinoma

All mice used in the study were 8-12 weeks old at the beginning of the experiments. For all animal experiments, cells were harvested using trypsin-EDTA, neutralized with FBS-containing media, and re-suspended in Hank's balanced salt solution (Gibco) before injection into the mice. To generate ovarian carcinoma models,

OVCAR5 cells (1 x 10^6 in 200 μL of Hank's balanced salt solution) and SKOV3ip1 cells (1 x 10^6 in 200 μL of Hank's balanced salt solution) were injected into mice intraperitoneally. Mice were given paclitaxel (35ug per mouse) once weekly or B-20-4.1.1 (VEGF:5563, Lot #71943-30, Genentech) (6.25 mg/kg) twice weekly via intraperitoneal injection. Furthermore, an empty DOPC liposome or L-Grb2 (BP1001-002; Bio-Path Holdings, Inc.) was injected intravenously via the tail vein at a dose of 15 mg/kg twice weekly. Once mice in any group became moribund, all mice were sacrificed. All animal studies were approved by MD Anderson IACUC committee. Tumors were harvested from the mice and weighed, and the numbers of nodules and tumor weights were recorded. Tumor tissue was preserved and fixed in formalin for paraffin embedding, frozen in optimal cutting temperature medium to prepare frozen slides, or snap-frozen for lysate preparation.

3.5 Immunohistochemistry

Harvested tumor samples were embedded in paraffin blocks and sectioned by the MD Anderson Research Histology Core Laboratory. Paraffin-embedded tissue samples were used to stain for Ki67 (RB-9043-P1; Thermo Fisher Scientific) and cleaved caspase-3 ([CC3]; 9661; Cell Signaling Technology). Briefly, sections of the samples were deparaffinized sequentially in xylene and decreasing concentrations of ethanol prior to rehydration and transfer to PBS. For CC3 antigen retrieval from the slides were placed in a steamer (Hamilton Beach) in sodium citrate (pH 6) buffer for 25 minutes. Antigen retrieval for staining for Ki67 was performed in Diva Decloaker solution (#DV2004MX; Biocare Medical). Endogenous tissue peroxidase activity was quenched with 3%

hydrogen peroxide in 100% methanol for 12 minutes. Slides were then washed and blocked with 5% goat serum in PBS for 1 hour at room temperature. A primary antibody was then diluted in 5% goat serum in PBS overnight at 4°C in a humidified chamber. Ki67 was diluted at 1:200, whereas CC3 was diluted at 1:100. Slides were then washed three times with PBS. CC3 stained slides were incubated with a biotinylated anti-rabbit antibody (#GR602H; Biocare Medical) for 20 minutes at room temperature. Next, slides were washed three more times with PBS and incubated for 20 minutes with a streptavidin-horseradish peroxidase label (#HP604H; Biocare Medicare). For Ki67 staining, slides were incubated with a secondary anti-rabbit antibody conjugated to horseradish peroxidase (#111-036-047; Jackson ImmunoResearch) diluted in 5% goat serum in PBS at a 1:500 dilution for 1 hour at room temperature. CD31 staining of frozen sections was also performed. Sections were fixed in cold acetone for 15 minutes, washed with PBS, blocked with 5% goat serum in PBS, and incubated with a rat monoclonal anti-mouse CD31 antibody (1:200, 553370; Pharmingen) overnight at 4°C. The next day, slides were washed with PBS, and an appropriate horseradish peroxidase-conjugated secondary antibody was placed on them for 1 hour at room temperature. After secondary antibody incubation, slides were again washed with PBS, briefly washed with PBS containing Brij 35 (#858366; Sigma-Aldrich), and placed in 3,3'-diaminobenzidine (#750118; Thermo Fisher Scientific). Upon color change, slides were rinsed in Milli-Q water and counterstained with hematoxylin (#GHS316; Sigma-Aldrich) for 13 seconds, rinsed in water again, and left to dry. Slides were then mounted with coverslips using Permount medium (#SP15-100; Thermo Fisher Scientific). Slides were imaged using a Leica DM4000 B LED microscope. For quantification of tumor specimens five random

high-power field (HPF) photographs of each slide were taken, and stained cells were counted manually.

3.6 EdU incorporation assay, annexin V staining, and cell-cycle assay

Ovarian cancer cells were plated in technical duplicates per experiment in six-well plates at a density of 50,000-100,000 cells per well. The next day, cells were transfected with siRNA as described above. SiGrb2 and siControl cells were harvested 72 hours after transfection. Harvested cells were then pulsed with EdU for 2 hours and processed using a Click-iT Plus EdU Alexa Fluor 488 Flow Cytometry Assay Kit (#C10632; Thermo Fisher Scientific) following the manufacturer's protocol. For annexin V staining ovarian cancer cells after transfection a BD Biosciences FITC Annexin V Apoptosis Detection Kit I (#556547) was used according to the manufacturer's protocol. After annexin V analysis, cells were stained with 4',6-diamidino-2-phenylindol) for use in cell-cycle analysis. For flow cytometric analysis and data collection a Beckman Coulter Gallios Flow Cytometer was used.

3.7 Colony formation assay

Ovarian cancer cells were plated in technical duplicates per experiment in six-well plates at a density of 1000 cells per well. Twenty-four hours after seeding, cells were transfected with either siControl or siGrb2 using methods described previously. Cells were left to grow in a tissue culture incubator for 7-10 days. Afterward, the cells were washed two times with ice-cold PBS and fixed with ice-cold 100% methanol for 10 minutes. After 10 minutes, the methanol was discarded, and the cells were stained with

a crystal violet solution (0.5% crystal violet with 20% methanol in Milli-Q water; Sigma-Aldrich) for 10 minutes at room temperature. Crystal violet was then removed, and the cells were washed with deionized Milli-Q water three times and left to dry at room temperature.

3.8 Invasion assay

Invasion assays were performed using a Transwell system (8-μm pore size; Corning Inc.). Briefly, 24 and 48 hours after siRNA transfection of Grb2 and control siRNA, cells were harvested and quantified. Next, 3 x 10^5 cells were seeded onto the apical side of a Transwell chamber pre-coated with Matrigel (six-well insert) in serum-deprived culture Media supplemented with 10% FBS was added to the basal compartment of the chamber to serve as a chemoattractant. The cells were allowed to migrate from top chamber to bottom chamber overnight for 24 hours and then fixed. The cells that remained on the apical side of the chamber were gently scraped off with cotton swabs. The invading cells were then quantified.

3.9 Tube formation assay

RF-24 endothelial cells were plated on six-well plates at a density of 100,000 cells per well and allowed to attach overnight. The cells were transfected with siControl or siGrb2 at 24 hours. After 72 hours, cells were harvested and counted. A μ-plate for use in an angiogenesis assay was then coated with 10 μL of Matrigel, which was allowed to solidify at 37°C for 1 hour. Next, 20,000 cells per well were seeded on the Matrigel. The cells were incubated at 37°C for 6 hours. To assess endothelial cell tube formation, we

counted and photographed complete tubes in randomly chosen fields at 40x magnification using an Olympus inverted microscope connected to a digital camera.

3.10 Ex-vivo NMR metabolomics

Excised tumor tissue samples were flash frozen, weighed and crushed into fine powder in liquid nitrogen environment. These were immersed in 3 mL of methanol-to-water solution (2:1) and vortexed in presence of polymer beads. A rigorous process of mechanical homogenization was followed by centrifugation of the solution for ten minutes to separate the water-soluble metabolites from proteins and other cellular constituents. [59] Rotary evaporation method was used for the supernatant to remove the methanol. A lyophilizer was used to dry the sample out and collect the metabolites. The water soluble metabolites were finally dissolved in a solution of 600 µL of $2H_20$, 36 µL of PO_4 buffer, and 4 µL of 80 mM DSS (4,4-dimethyl-4-silapentane-1-sulfonic acid). Phosphate buffer was added to stabilize the pH variations, and DSS was served as the reference standard to normalize the spectroscopic NMR signal of each metabolite. [60]

NMR spectrum of each sample was obtained using a Bruker AVANCE III HD® NMR scanner (Bruker Bio Spin Corporation, at room temperature The operating frequency of the NMR spectrometer for proton resonance was 500 MHz and it was endowed with a triple resonance (^1H, ^{13}C, ^{15}N) cryogenic temperature probe with a Z-axis shielded gradient. Water suppression sequence was employed using a pre-saturation technique of the RF pulse. Spectroscopic data were obtained with a 90º pulse width flowed a scan delay t_{rel} of 6.0 s, a 1024 Hz spectral width. The time domain NMR signal was acquired using an exponential function. After the final spectrum was acquired the phase correction

was performed. The analysis of the metabolomics data was carried out using Chenomx NMR Suite 8.1 software (Chenomx Inc., Edmonton, Canada). Quantitative analysis of the metabolites was then performed using MestReNova software (Mestrelab Research, Spain) by integrating the resonance peak for each metabolite. Finally the integral value was normalized by the value of the integral of the DSS resonance peak.

3.11 Reverse phase protein array and pathway analysis

A reverse phase protein array (RPPA) assay was carried out by the MD Anderson Functional Proteomics Reverse Phase Protein Array (RPPA) Core. OVCAR8 cells were treated with siControl or siGrb2 for 72 hours. Cell lysates were then collected in RIPA buffer containing freshly added protease and phosphatase inhibitors. Protein concentrations were quantified using a BCA assay kit (Pierce Biotechnology), and 45 μg of protein from each group was used for RPPA analysis with a validated set of antibodies. To determine the biological function of Grb2, protein expression changes after siRNA transfection were used for pathway analysis with Ingenuity Pathway Analysis software and Netwalker pathway analysis software. The comparison analysis between siControl-treated cells and siGrb2-treated cells was carried out in R (version 3.5.1). Normalized data was at first log2 transformed (log2(x+1)). Differential expressed proteins between the two groups were identified by a p-value, obtained from the moderated t-statistic from LIMMA package, of less than 0.05. To support visual data exploration, a heatmap for the most significant cases was generated using the heatmap.2 function from the gplots package.

3.12 Statistical analysis

The Student *t*-test (for comparison of two groups) and ANOVA (for comparison of all groups) were used to calculate *P* values for normally distributed data. Network and pathway analyses were performed using the NetWalker network analysis (version 1.0) and Ingenuity Pathway Analysis software programs. All statistical data were analyzed using the Prism software program (GraphPad Software). *P* values less than 0.05 according to two-tailed tests were considered significant. When multiple tests were performed, the BUM (beta uniform mixture) model [61] was used to fit p-values and estimate counts of significant features at different FDRs. All statistical tests were two-sided unless otherwise noted.

4. Results

4.1 Therapeutic Efficacy of L-Grb2 in Orthotopic models of ovarian cancer

We first performed an L-Grb2 dose-finding experiment using a murine ovarian cancer model (OVCAR5) and measured Grb2 protein expression in harvested tumors at 24 and 72 hours after L-Grb2 administration. Grb2 protein expression was reduced in tumors for up to 72 hours after injection of 15 and 25 mg/kg L-Grb2 **(Figure 4).** Next, we examined the effects of 15 and 25 mg/kg L-Grb2 on tumor growth *in vivo* using the OVCAR5 model. After intraperitoneal injection of OVCAR5 cells, we gave mice L-Grb2 twice weekly. We observed a reduction in tumor growth at 15 mg/kg, but there was no additive benefit of increasing the L-Grb2 dose beyond that. We also saw a reduced number of nodules after treatment with 15 mg/kg L-Grb2. Weight loss did not differ markedly among the treatment groups **(Figure 4B-E)**. First line chemotherapy in ovarian cancer patients includes platinum- and taxane- based therapy. Since taxanes have combined well with biologically targeted drugs, we first performed a series of experiments to characterize the therapeutic efficacy of L-Grb2 in combination with paclitaxel. In the OVCAR5 model, tumor growth was significantly lower in mice given L-Grb2 and paclitaxel (0.17 g ± 0.10 g) than in control mice (0.99 g ± 0.35 g) **(Figure 5A).** We noted a decrease in tumor growth in the mice given L-Grb2 only, as well (0.29 g ± 0.14 g). We observed fewer metastatic nodules in mice given L-Grb2 only or combined with paclitaxel than in control mice given an empty DOPC liposome (L-Grb2 only, 5.9 ± 2.9; L-Grb2 and paclitaxel, 2.00 ± 0.72; control, 9.2 ± 2.5) **(Figure 5B).** We noted no changes in mouse weight and no noticeable changes in mouse mobility during treatment with L-Grb2 **(Figure 4E).**

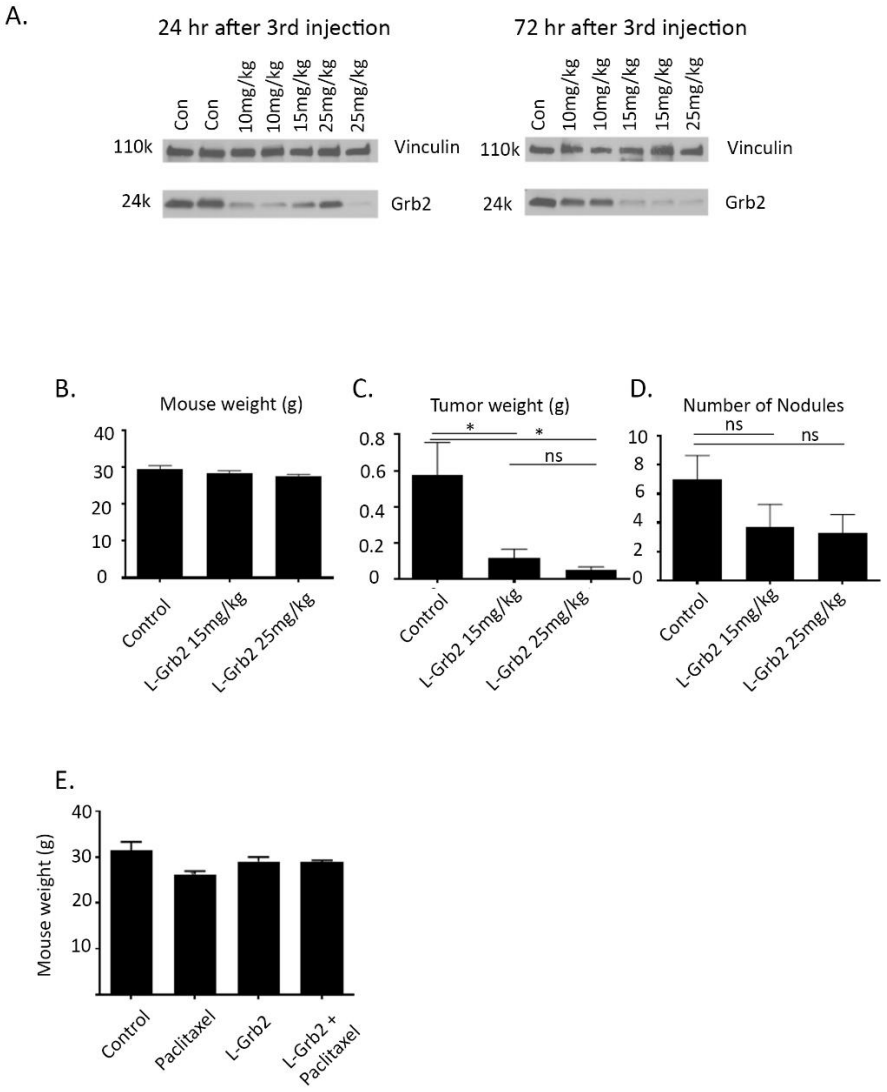

Figure 4. Results of an L-Grb2 dose-defining experiment to evaluate ovarian tumor growth. **A,** Western blot analysis of Grb2 protein expression in tumors obtained from mice inoculated with OVCAR5 cells 24 and 72 hours after the last intravenous injection of an empty DOPC liposome (control [Con]), 10 mg/kg L-Grb2, 15 mg/kg L-Grb2, or 25 mg/kg L-Grb2. **B-D,** Mean body weights of (**B**), tumor weights in (**C**), and numbers of metastatic nodules in (**D**) mice intraperitoneally inoculated with OVCAR5 cells (*n* = 10 per group). Mice received treatment with L-Grb2 at 15 and 25 mg/kg twice weekly. **E,** Mean body weights of mice inoculated with OVCAR5 cells that received control treatment, paclitaxel only (3 mg/kg) weekly, L-Grb2 only (15 mg/kg) twice weekly, or a combination of L-Grb2 and paclitaxel beginning 10 days after inoculation (*n* = 9 mice per group). Error bars, SEM. All statistical tests were two-sided. Asterisk indicates statistical significant of ***p<0.001, **p<0.01, *p<0.05. NS indicates non-significant.

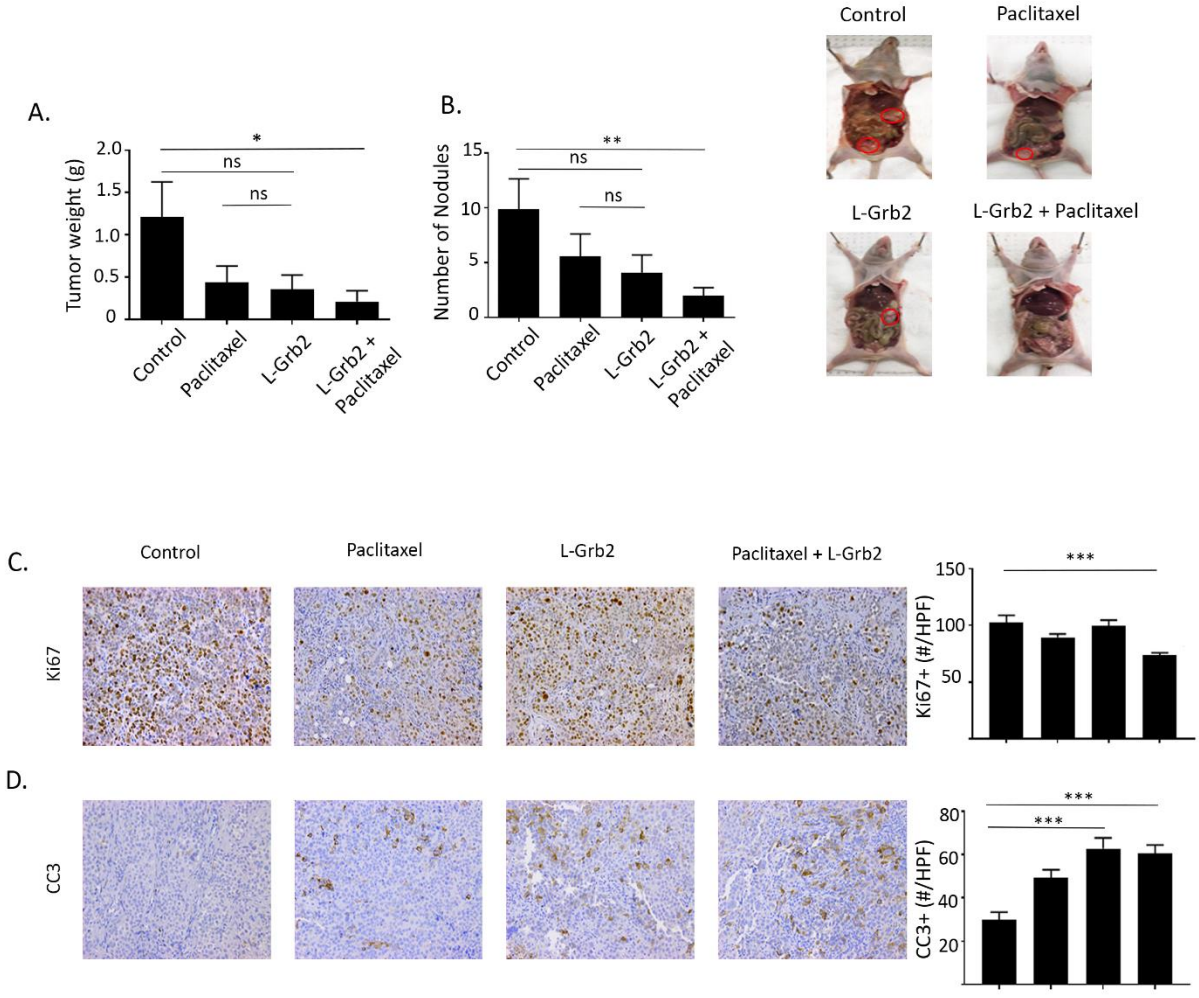

Figure 5. Effects of treatment with L-Grb2 on ovarian tumor growth. **A and B,** Mean tumor weights (**A**) and numbers of metastatic nodules (**B**) in mice intraperitoneally inoculated with OVCAR5 cells that received an empty DOPC liposome (control), paclitaxel only (3 mg/kg) weekly, L-Grb2 (15 mg/kg) twice weekly, or a combination of L-Grb2 and paclitaxel beginning 10 days after inoculation (*n* = 9 mice per group). **C and D,** Tumors collected from the mice at the conclusion of *in vivo* therapeutic experiments and tumors were examined using immunohistochemical staining to evaluate the effects of treatment with L-Grb2, paclitaxel, or both in comparison with those of the control treatment on (**C**) cell proliferation (Ki67 staining) and (**D**) apoptosis (CC3 staining). Representative images of mice from the four groups taken at 20x magnification are shown at the upper right. The mean numbers of Ki67+ and CC3 + cells per group are shown in the adjoining graphs. Five tumors per group were stained, and five representative images per sample were quantified were used for analysis. Error bars, SEM. All statistical tests were two-sided. Asterisk indicates statistical significant of ***p<0.001, **p<0.01, *p<0.05. NS indicates non-significant.

4.2 Biological effects of L-Grb2 on proliferation and apoptosis

Ovarian tumors harvested from mice in our *in vivo* experiments were then stained for markers of proliferation (Ki67) and apoptosis (CC3). In the OVCAR5 model, treatment with the combination of L-Grb2 and paclitaxel resulted in the greatest reduction of cellular proliferation as determined via Ki67 staining (mean, 73.50 Ki67+ cells per HPF). In comparison, the mean numbers of Ki67+ cells per HPF were 102.40 in the control group, 89.43 in the paclitaxel-alone group, and 99.95 in the L-Grb2–alone group **(Figure 5C)**. In addition, we saw more CC3+ cells in the L-Grb2–alone (mean, 62.82 CC3+ cells per HPF) and combination L-Grb2 and paclitaxel (mean, 60.55 CC3+ cells per HPF) groups than in the control (mean, 29.95 CC3+ cells per HPF) and paclitaxel-alone (mean, 49.30 CC3+ cells per HPF) groups **(Figure 5D)**. The reduction in number of proliferative cells and increase in that of apoptotic cells were significant in the combination group compared to control groups.

4.3 Effect of Grb2 downregulation in ovarian cancer cell lines *in vitro*

We measured the baseline expression of Grb2 in a panel of seven ovarian cancer cell lines and compared it with that in the non-transformed ovarian cell line HIO180 **(Figure 6A)**. We then transfected the cells with 100nm of siControl or siGrb2 to downregulate Grb2 protein expression **(Figure 6B)**. After observing decreased protein expression of Grb2 in all cell lines, we assessed the effect of Grb2 downregulation on three cell lines with high Grb2 protein expression (OVCAR8, OVCAR5, and SKOV3ip1) and two with low Grb2 protein expression (HEYA8 and A2780) using a cell viability assay. OVCAR8

and SKOV3ip1 were the most sensitive to Grb2 downregulation **(Figure 6C and D)**. We characterized the cell lines according to their mutation status and found that cell lines with ErbB2 mutations or amplifications were the most sensitive to Grb2 downregulation **(Table 3)**. Increased ErbB2 protein expression was confirmed on Western blot analysis **(Figure 6E).**

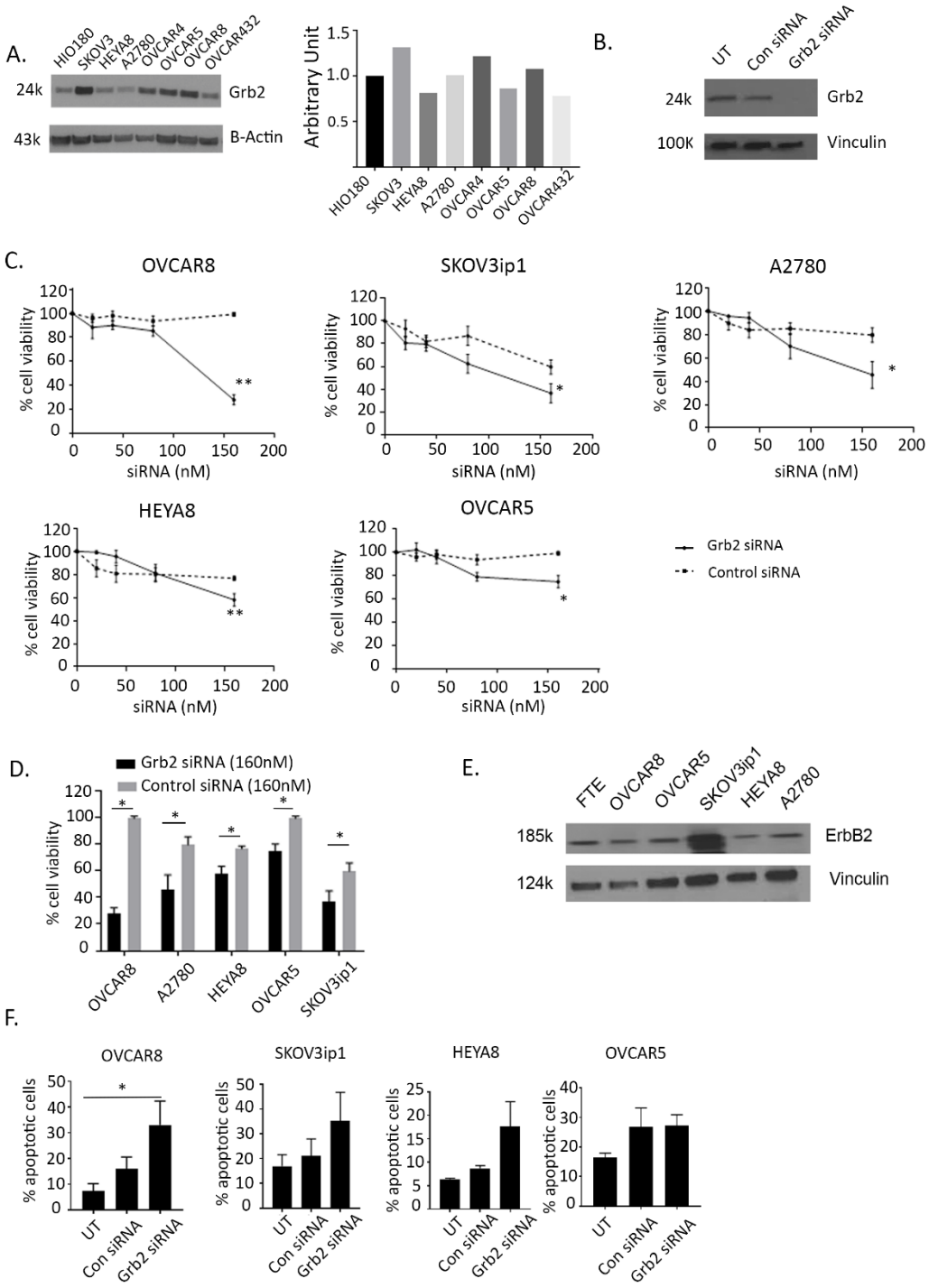

Figure 6. Effect of Grb2 downregulation on ovarian cancer cell lines. **A,** Western blot analysis of Grb2 expression in a panel of ovarian cancer cell lines compared with that in the non-transformed epithelial ovarian cell line HIO180. The adjoining graph shows their expression compared with that in HIO180. **B,** Western blot analysis of Grb2 expression in OVCAR8 cells 72 hours after siGrb2 transfection compared with that in untreated (UT) and siControl-transfected (Con siRNA) cells. **C,** OVCAR8, SKOV3ip1, A2780, HEYA8,

and OVCAR5 cell lines were transfected with siGrb2 or siControl at increasing concentrations. An alamarBlue assay of the cells was performed 72 hours after transfection to determine their percent viability, which is shown in the graphs. The data represent averages of triplicate measurements. **D,** The percent viability of the five cell lines in **C** 72 hours after transfection of siGrb2 and siControl at 160 nM. **E,** Western Blot analysis of ErbB2 expression in a panel of ovarian cancer cell lines compared to fallopian tubal epithelium (FTE) **F,** Results of an annexin V assay performed to determine the number of apoptotic untreated (UT), siControl-transfected (100 nM), and siGrb2-transfected (100 nM) ovarian cancer cells. The assay was performed 72 hours after transfection. Error bars, SEM. All statistical tests were two-sided. Asterisk indicates statistical significant of ***p<0.001, **p<0.01, *p<0.05. NS indicates non-significant.

Table 3. Mutation statuses of the ovarian cancer cell lines used in the study [62,63]

	Gene				
Cell line	**ErbB2**	**PIK3CA**	**PTEN**	**KRAS**	**BRAF**
OVCAR-8	Mut	WT	WT	Mut	WT
A2780	WT	Mut p.E365K	Mut p.KGR128del	WT	Mut
OVCAR-5	WT	WT	WT	Mut pG12V	WT
HeyA8	WT	WT	WT	Mut	Mut
SKOV3ip1	Amp	Mut p.H1047R	WT	WT	WT

Abbreviations: Amp, amplification; Mut, mutant; WT, wild-type.

Because of the inhibition of ovarian tumor growth and increased apoptosis in *in vivo* tumor specimens, we next examined the *in vitro* effects of Grb2 downregulation by siRNA

on the ovarian cancer cell lines described above. An annexin V assay demonstrated an increase in apoptosis after Grb2 downregulation in all cell lines, with the greatest effects seen in the OVCAR8 cells (siGrb2**,** 33.0% apoptotic; untreated, 7.3% apoptotic) and SKOV3ip1 cells (siGrb2, 17.69% apoptotic; untreated, 6.41% apoptotic) **(Figure 6F).** Next, we examined the effect of Grb2 downregulation on ovarian cancer cell proliferation. We observed no effect on the number of proliferative OVCAR8 cells at 72 hours (siControl, 34.95 ± 0.94; siGrb2, 37.94 ± 1.54) **(Figure 7A).** We also observed no change in the number of colonies formed in OVCAR5 cells in a colony formation assay (siControl, 848 ± 53; siGrb2, 1014 ± 121). However, the quantified colonies were smaller in the siGrb2-exposed group than in the controls (mean ± SEM colony area: siGrb2, 1.290 ± 0.175 mm^2; siControl, 2.45 ± 0.50 mm^2) **(Figure 7B**). These results corroborated our *in vivo* findings that Grb2 downregulation due to treatment with L-Grb2 leads to an increase in the number of apoptotic cells. We found no effects of Grb2 downregulation on cell-cycle progression **(Figure 8A).** Finally, we performed an invasion assay using OVCAR8 cancer cells at varying time points. At 72 hours after transfection we found cells treated with siGrb2 were largely apoptotic. At 48 hours, cells treated with siGrb2 were found to have no effect on invasive potential **(Figure 8B)**.

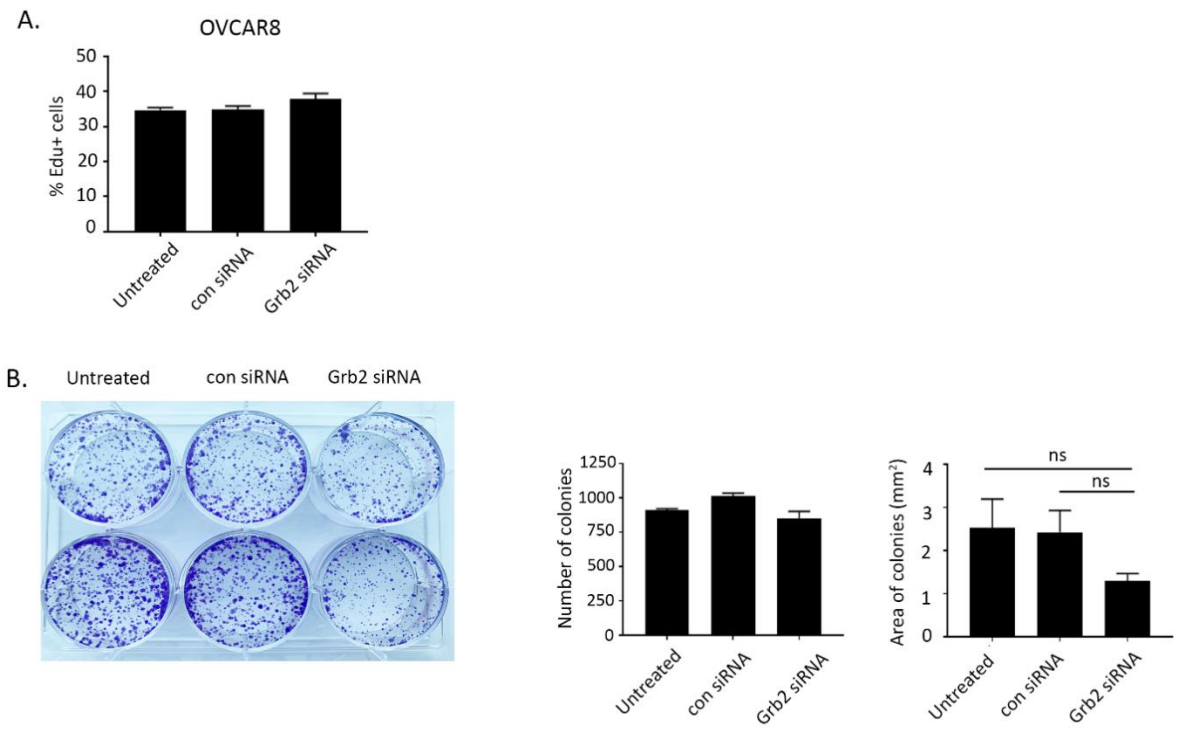

Figure 7. Effect of Grb2 downregulation on ovarian cancer cell proliferation. **A,** Results of an EdU incorporation assay performed to determine the number of proliferative untreated, siControl-treated (con), and siGrb2 treated OVCAR8 cells (72 hours after treatment). **B,** Results of a colony formation assay of the OVCAR5 cell line. After siRNA-based treatment, cell colonies were allowed to grow for 7-10 days before quantification. The adjoining graph shows the mean ± SEM total number of colonies and area of colonies in the three groups. Asterisk indicates statistical significant of ***p<0.001, **p<0.01, *p<0.05. NS indicates non-significant.

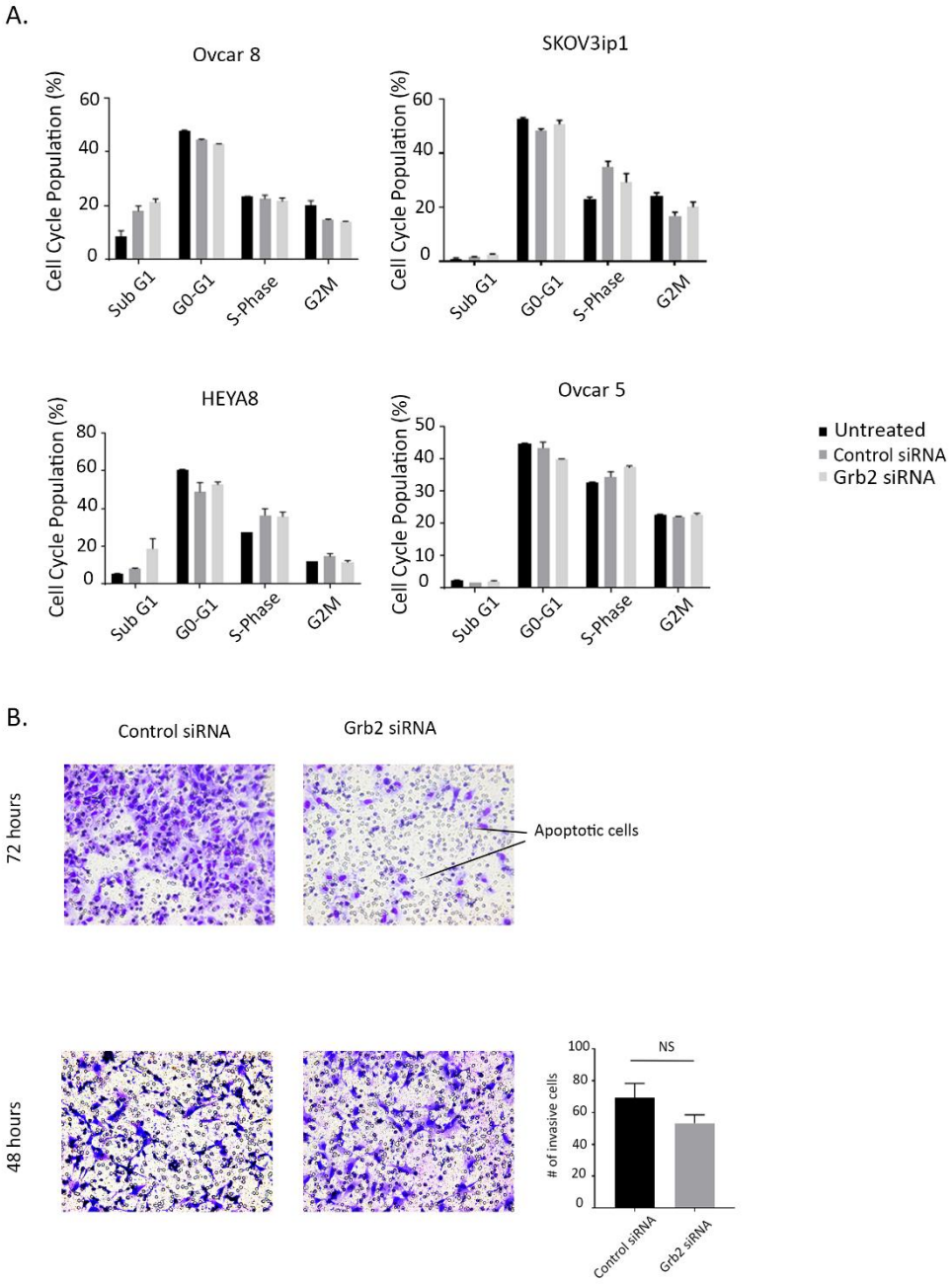

Figure 8. Effect of Grb2 downregulation on cell-cycle progression and invasion in ovarian cancer cells. **A,** Results of a cell-cycle assay performed using untreated, siControl-treated, and siGrb2-treated OVCAR8, SKOV3ip1, HEYA8, and OVCAR5 cells at 72 hours after transfection. **B,** Results of a Matrigel invasion assay performed 48 and 72 hours after transfection of OVCAR8 ovarian cancer cells with siControl or siGrb2. At 72 hours, cells were apoptotic, and quantification **of** invading cells was not performed. The adjoining graph shows the corresponding mean numbers of invasive cells 48 hours after transfection. Error bars, SEM. All statistical tests were two-sided. Asterisk indicates statistical significant of ***p<0.001, **p<0.01, *p<0.05. NS indicates non-significant.

4.4 Pathway analysis after Grb2 downregulation on ovarian cancer cell lines

Next, to understand the broader downstream effects of Grb2 inhibition on ovarian cancer cell lines we conducted an RPPA analysis with OVCAR8 cells **(Figure 9A).** To identify pathways in these cells affected by Grb2 downregulation after transfection with siGrb2, we used the NetWalker software program **(Figure 9B).** Networks significantly affected by Grb2 downregulation included *Generation of precursor metabolites and energy* (downregulated) and *Negative regulation of apopt*osis (downregulated) **(Table 4).** Additionally, there was downregulation of insulin receptor signaling **(Table 4)** and glycolytic metabolites **(Figure 9C).** We confirmed the protein expression of glycolytic enzymes and marker of mitochondrial stress, superoxide dismutase 2 (SOD2), by Western blot **(Figure 9D).** It is well documented that rapidly proliferating tumor cells rely on aerobic glycolysis in a phenomenon referred to as the Warburg effect [64-66]. Deregulated c-MYC, HIF1a and growth signaling lead to induction of glycolytic enzymes and inhibition of pyruvate oxidation in mitochondria [67-69]. Disrupting the Warburg effect to shunt cancer metabolism to oxidative phosphorylation, subsequently increases oxidative stress triggering apoptosis [70-72]. Therefore, based on our RPPA and pathway analysis we hypothesized Grb2 downregulation was leading to a disruption in the Warburg effect, shunting metabolism to the tricarboxylic acid (TCA) cycle. To confirm this, we performed metabolomic analysis of OVCAR8 cells with Grb2 downregulation. Specifically, we compared the metabolite levels in OVCAR8 cells transfected with siControl to those cells transfected with siGrb2. We analyzed a total of 295 metabolites and found that 61 of them were significantly dysregulated after Grb2 downregulation **(Figure 10A).** We then performed metabolite set enrichment analysis of the relative

concentrations of metabolites with significant differences between OVCAR8 cells with Grb2 downregulation and control cells to identify biological patterns **(Figure 10B).** Additionally, we used the metabolomic pathway analysis module of the MetaboAnalyst software program to identify the pathways most affected by Grb2 downregulation. Dysregulated metabolites lead to enrichment of amino acid metabolism and the TCA cycle **(Figure 11A).** Because pathway analysis could only provide associations between metabolites and pathway regulation, we went back to our original data to quantify metabolites specific to the TCA cycle. We found an increase in TCA intermediates, fumurate, malate, succinate, isocitrate, succinyl-coA and oxaloacetate in cells transfected with siGrb2 **(Figure 11B).** Finally, we corroborated these results with our harvested *in vivo* tumors through NMR spectroscopy. After tumors were analyzed, metabolite levels between L-Grb2 and empty DOPC treated tumors were compared. We found substantially lower lactate and choline levels in the L-Grb2 monotherapy group of tumors harvested than in the control group **(Figure 11C, Figure 12).** Based on these findings we concluded that Grb2 downregulation leads to a disruption of the Warburg effect though a decrease in LDHA. This subsequently increases oxidative phosphorylation, and mitochondrial stress as seen through an increase in SOD2.

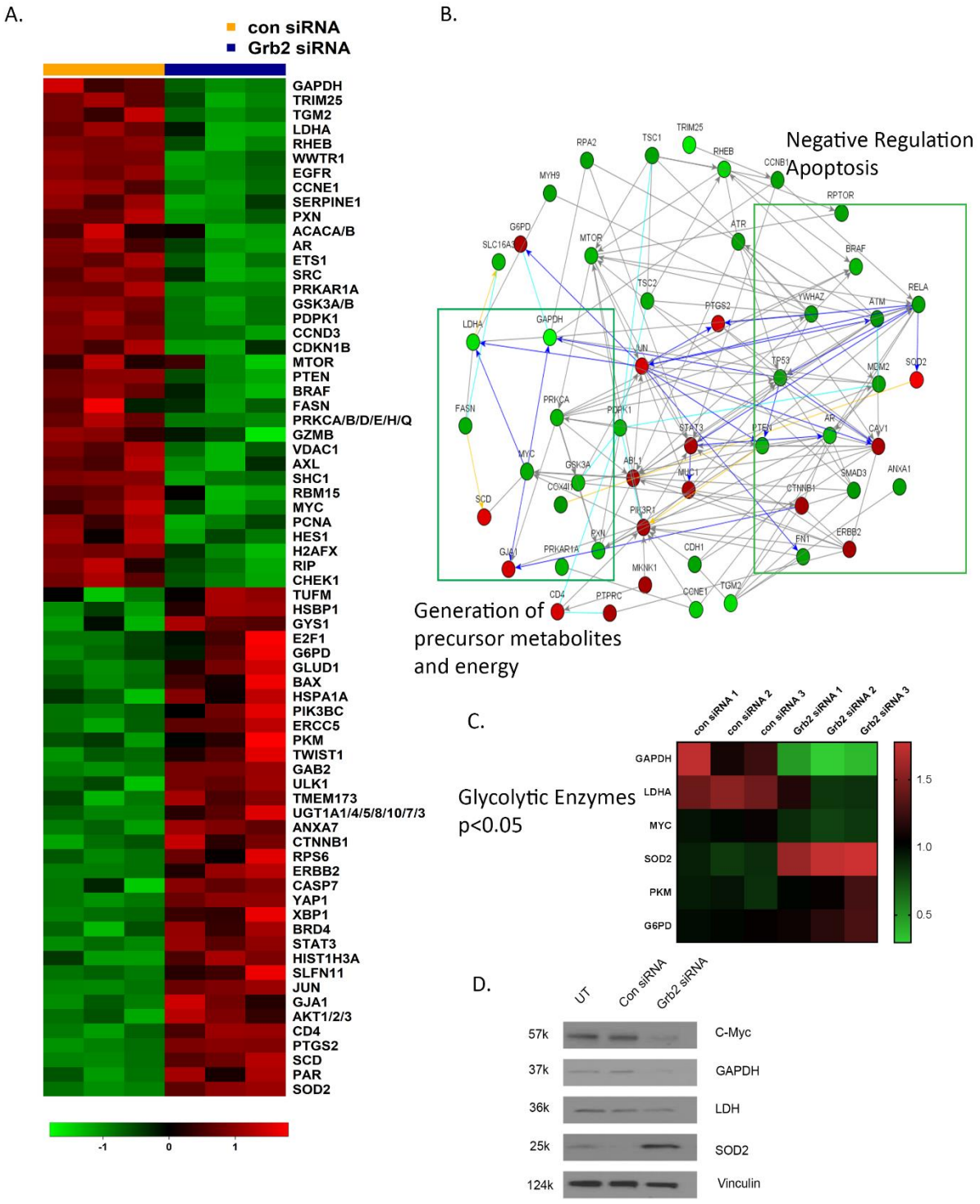

Figure 9. Differential expression of proteins OVCAR8 ovarian cancer cells after Grb2 downregulation as detected using an RPPA. **A,** Heat map of proteins whose expression differed significantly between siGrb2- and siControl-transfected groups ($P < 0.05$). **B,** Networks generated after Grb2 downregulation using NetWalker software. Fold changes

in protein expression were calculated on the basis of NormLog2 expression differences between the siControl- and siGrb2-transfected cells. **C,** Heat map of glycolytic enzymes whose expression differed between siGrb2- and siControl-transfected groups (P<0.05). **D,** Western blot analysis of glycolytic enzymes after siGrb2 transfection.

Table 4. The networks most affected by Grb2 downregulation in ovarian cancer cells

Network	**Effect**	**Number of occurrences***
Cellular response to hormone stimulus	Downregulated	10
Response to insulin stimulus	Downregulated	9
Negative regulation of apoptosis	Downregulated	8
Generation of precursor metabolites and energy	Downregulated	7
Regulation of leukocyte activation	Upregulated	10
Hematopoiesis	Upregulated	10
T-cell activation	Upregulated	7
Regulation of kinase activity	Upregulated	7

*The number of molecules significantly associated with the network**.**

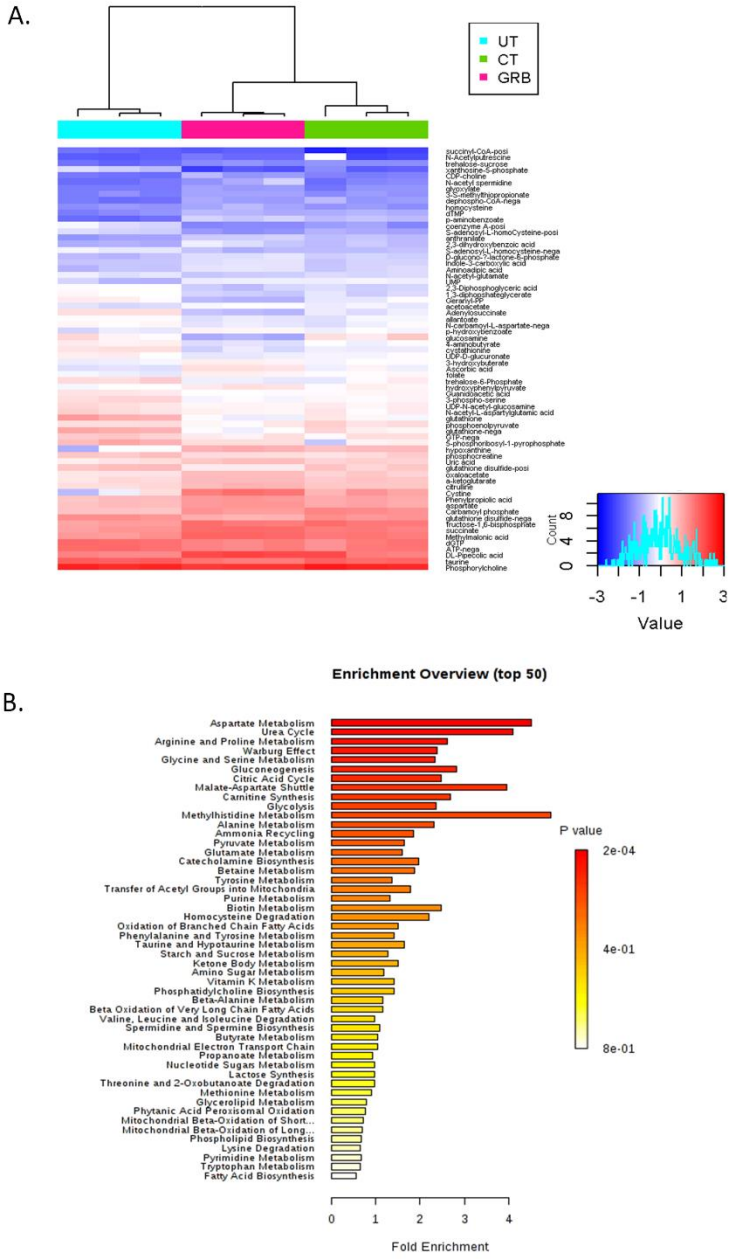

Figure 10. Effect of Grb2 downregulation on metabolite levels in ovarian cancer cells. OVCAR8 ovarian cancer cells harvested after control and Grb2 siRNA transfection. Cells then underwent mass spectroscopy for quantification of metabolites. **A,** Heatmap of 61 metabolites differentially expressed after Grb2 siRNA transfection. **B,** Pathways overrepresented in differentially expressed metabolites in siGrb2-transfected but not in siControl-transfected ovarian cancer cells. Metabolite set enrichment analysis was performed using the MetaboAnalyst software program.

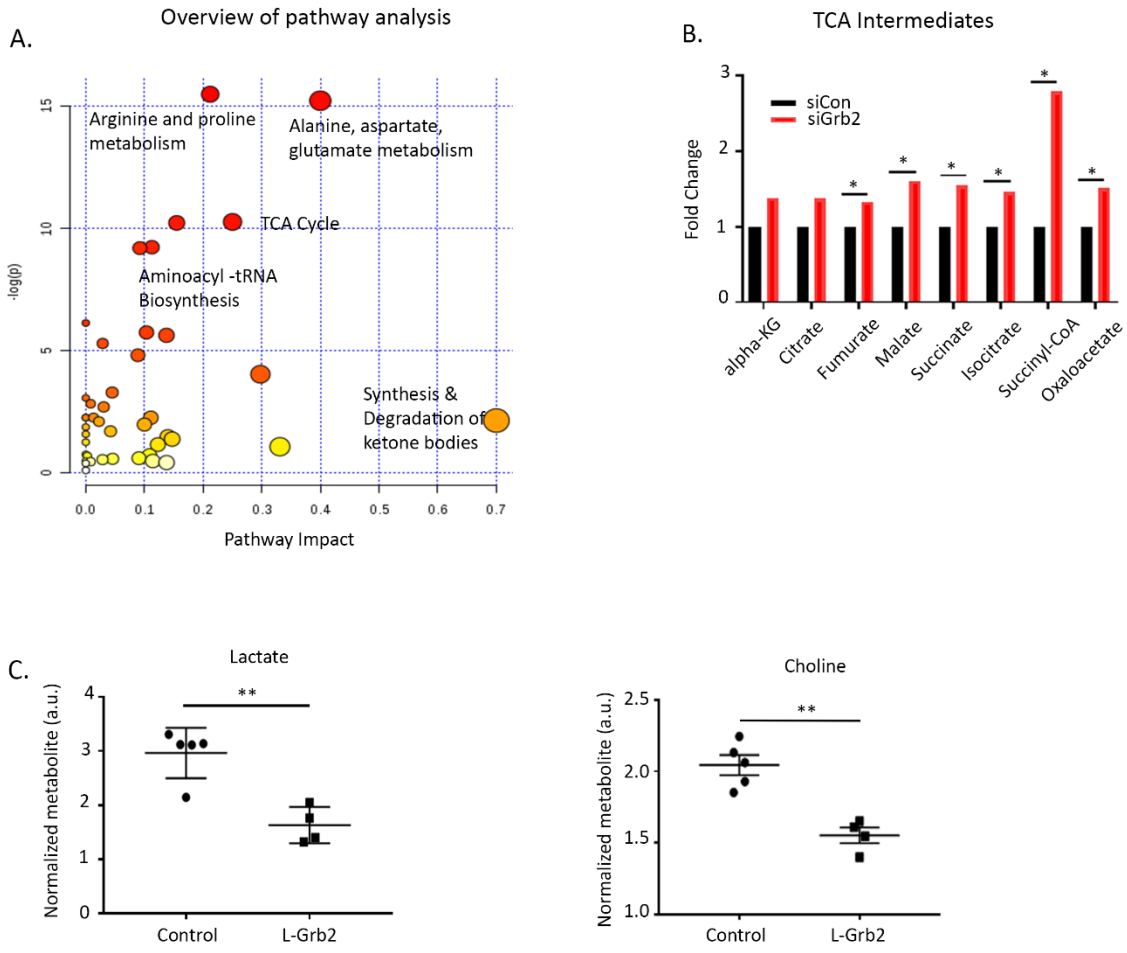

Figure 11. Effect of Grb2 downregulation on metabolite levels in ovarian cancer cells. **A,** Metabolites analyzed using the pathway analysis module of MetaboAnalyst. TCA, tricarboxylic acid; tRNA, transfer RNA. **B,** TCA metabolite levels in OVCAR8 ovarian cancer cells after siGrb2 and siControl transfection. **C,** Effect of Grb2 downregulation on lactate and choline levels in ovarian tumors. Mass spectroscopy was used to quantify metabolite levels in OVCAR5 tumors collected at the conclusion of an *in vivo* therapeutic experiment from control mice and mice given L-Grb2–based monotherapy (n = 5). Error bars, SEM. All statistical tests were two-sided. Asterisk indicates statistical significant of ***p<0.001, **p<0.01, *p<0.05. NS indicates non-significant.

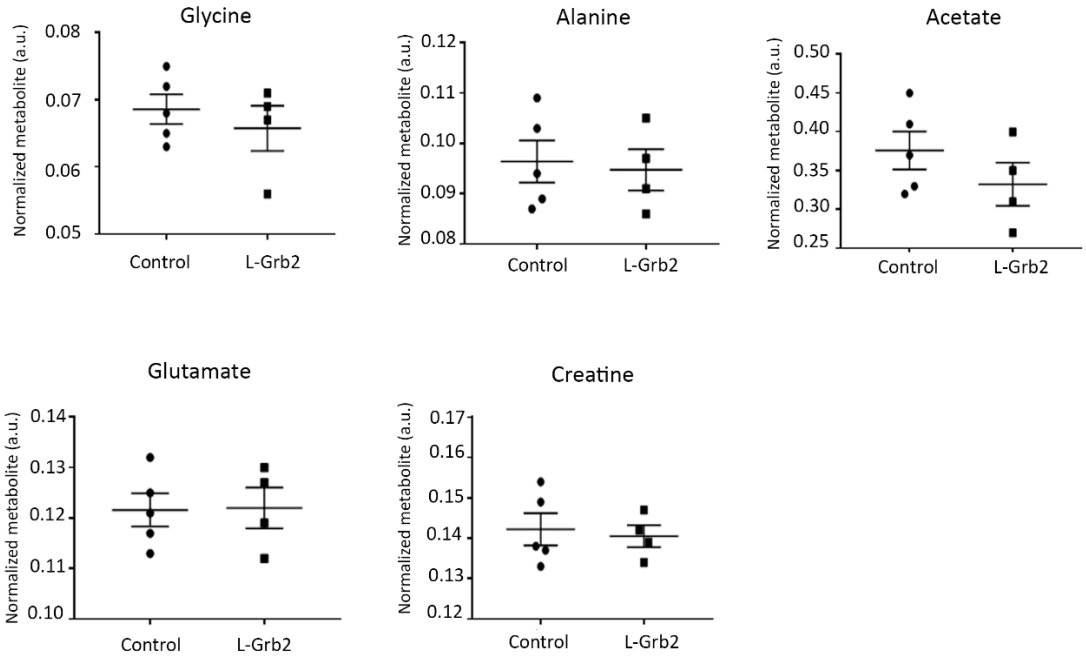

Figure 12. Effect of Grb2 downregulation on mean metabolite levels in ovarian tumors. Mass spectroscopy was used to quantify metabolite levels in OVCAR5 tumors collected at the conclusion of an *in vivo* therapeutic experiment from control mice and mice given L-Grb2–based monotherapy (*n* = 5). Error bars, SEM. All statistical tests were two-sided. Asterisk indicates statistical significant of ***p<0.001, **p<0.01, *p<0.05. NS indicates non-significant.

4.5 Anti-angiogenic effects of L-Grb2 and B-20 in ovarian tumors

The vascular endothelial growth factor (VEGF) signaling pathway plays a pivotal role in angiogenesis, thus several strategies have been designed to target VEGF signal transduction [73,74]. The effects of VEGF are mediated by two receptor tyrosine kinases, VEGFR-1 and VEGFR-2, which require Grb2 for signaling [75]. To investigate the relationship between Grb2 and angiogenesis through VEGF signaling we examined TCGA tumor mRNA expression. We found Grb2 expression correlates strongly with VEGFR-1 (R=0.61, P<0.001), VEGFR-2 (R=0.62, P<0.001), expression and pro-angiogenic genes E-Cadherin (R=0.51, P<0.001), and PECAM1 (R=0.75, P<0.001), **(Figure 13A).** Given these findings, we hypothesized that Grb2 downregulation may lead

to a decrease in angiogenesis and thus work well with anti-angiogenic therapy. To test this, we performed a cell viability assay and found a decrease in the number of viable RF-24 endothelial cells after Grb2 downregulation **(Figure 13B).** We then tested the effect of Grb2 downregulation on RF-24 cells *in vitro* using an endothelial cell tube formation assay **(Figure 13C).** We observed a decrease in endothelial cell viability with Grb2 downregulation and a corresponding decrease in the number of tubes formed by RF-24 cells (mean [± SEM], 19 ± 1 tubes for siGrb2-transfected cells and 76 ± 6 tubes for siControl-transfected cells).

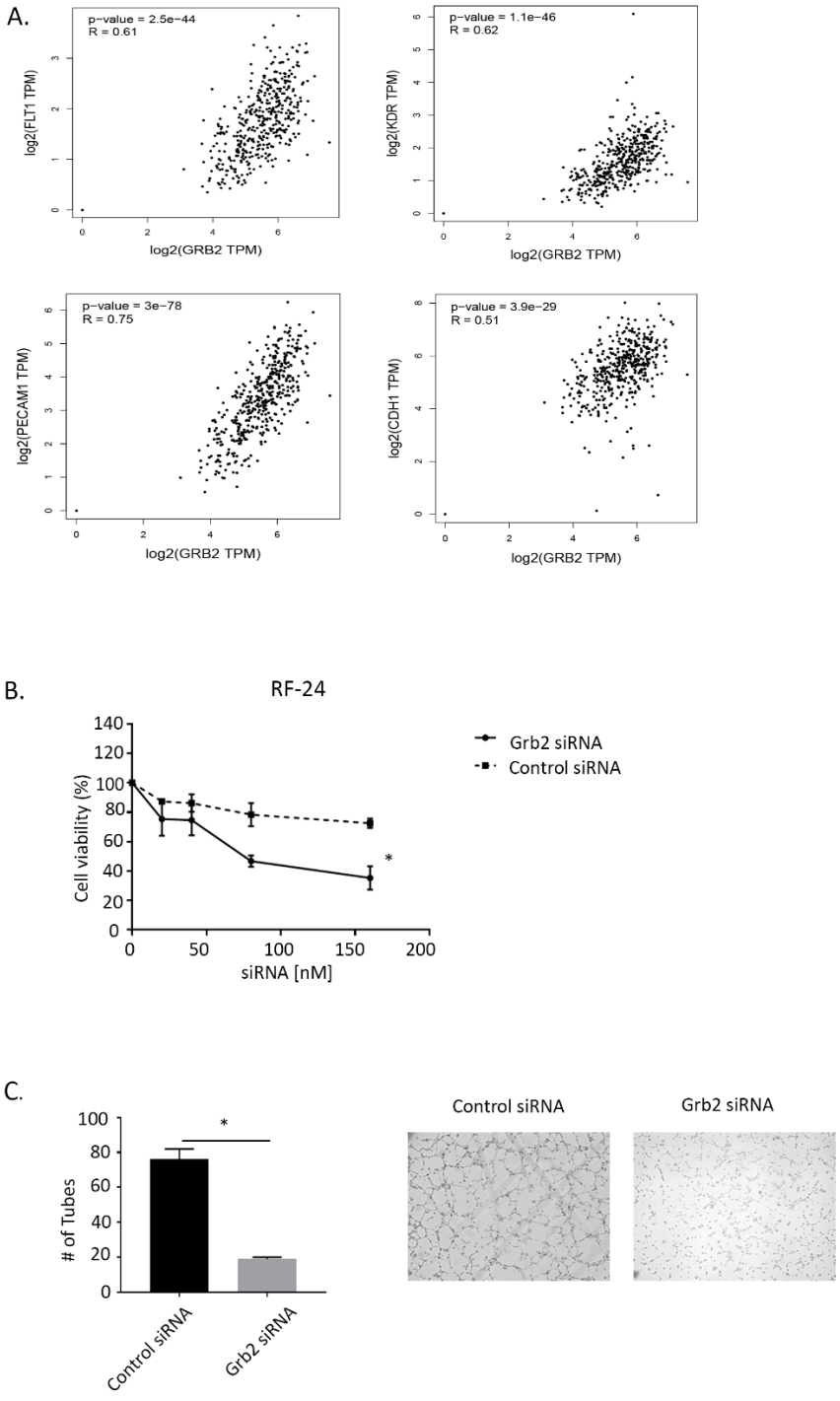

Figure 13. A. TCGA tumor mRNA seq expression data. Correlation between Grb2 expression and VEGFR1 (FLT1), VEGFR2 (KDR), PECAM1 and E-Cadherin (CDH1). **B-C.** *In vitro* effects of Grb2 downregulation on endothelial cells. **B,** Results of an alamarBlue viability assay performed to determine the sensitivity of siGrb2-transfected

RF-24 endothelial cells to Grb2 downregulation versus that of siControl-transfected RF-24 cells. The assay was performed 72 hours after transfection. The data represent the average values from triplicate measurements. **C,** Left: the mean numbers of tubes formed **by** RF-24 cells on a gel matrix (*n* = 3 wells per group; mean number of tubes quantified using five pictures per well). Right: representative images of endothelial vessel formation of **by** RF-24 cells after transfection with siGrb2 or siControl. Images were taken at 40x magnification. Error bars, SEM. All statistical tests were two-sided. Asterisk indicates statistical significant of ***p<0.001, **p<0.01, *p<0.05. NS indicates non-significant.

Next, we evaluated the effects of L-Grb2 on angiogenesis *in vivo*. First, we investigated the effects of treatment with L-Grb2 in combination with B-20 in SKOV3ip1 cells. We also observed substantial reductions in tumor weight in all groups of mice, with a 86% decrease in tumor weight in mice given the combination of L-Grb2 and B-20 (mean ± SEM, 0.16 g ± 0.05 g versus 1.21 g ± 0.49 g in the control group). The number of tumor nodules was decreased in all groups. We also saw no significant differences in mouse weights in the treatment groups **(Figure 14A-C).** We then stained tumors harvested from the study mice for the vessel marker CD31. We found decreases in the number of vessels in all treatment groups, as the mean (± SEM) vessel numbers were 26.97 ± 3.37 in the control group, 11.28 ± 1.29 in the B-20–only group, 18.67 ± 2.84 in the L-Grb2–only group, and 10.38 ± 1.19 in the combination L-Grb2 and B-20 group **(Figure 14D).** We also stained OVCAR-5 tumor sections for CD31 and found a significantly lower mean (± SEM) number of vessels in mice given the combination of L-Grb2 and paclitaxel (34.11 ± 3.46) than in the L-Grb2–only (24.88 ± 3.88), control (33.33 ± 3.25), and paclitaxel-only (33.33 ± 3.25) groups **(Figure 14D).**

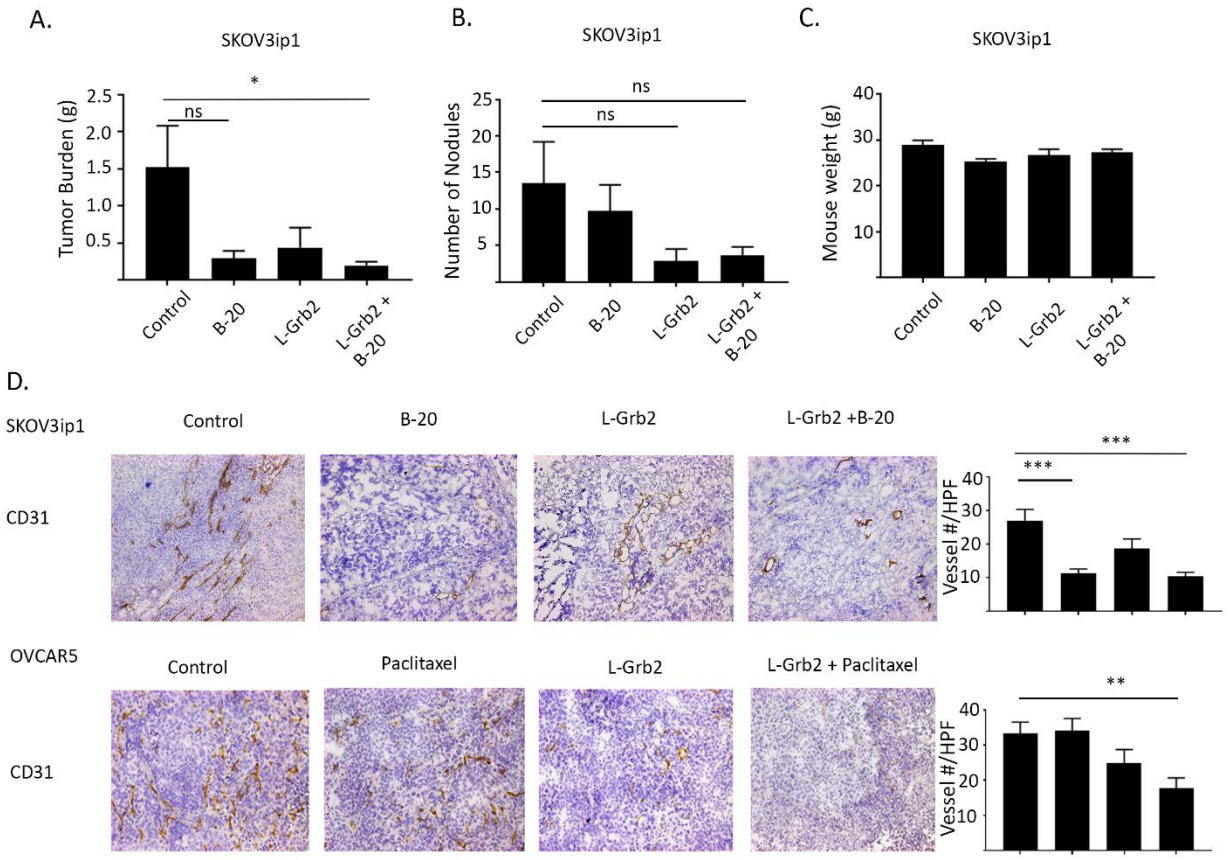

Figure 14. *In vivo* effects of treatment with L-Grb2 in combination with antiangiogenic therapy in an ovarian tumor model. **A-C,** Mean tumor weights in (**A**), numbers of metastatic nodules in (**B**), and body weights of (**C**) mice intraperitoneally inoculated with SKOV3ip1 cells that received control treatment, B-20 only (15 mg/kg) twice weekly, L-Grb2 only (15 mg/kg) twice weekly, or a combination of B-20 and L-Grb2 beginning 10 days after inoculation (*n* = 9 mice per group). **D,** Tumors collected from the SKOV3ip1 and OVCAR5 models at the conclusion of *in vivo* therapeutic experiments were subjected to immunohistochemical staining for CD31 to evaluate the effects on tumor vessel number of treatment with L-Grb2, B-20, or both compared with the control treatment. Representative staining images taken at 20x magnification are shown. The mean CD31+ cell numbers per group are shown in the adjoining graphs. Five tumors per group were stained, and five representative images per sample were quantified for analysis. Error bars, SEM. All statistical tests were two-sided. Asterisk indicates statistical significant of ***p<0.001, **p<0.01, *p<0.05. NS indicates non-significant.

4.6 Effect of Grb2 downregulation in uterine cancer cell lines *in vitro*

Next, we sought to determine the role of Grb2 in uterine cancer cell lines. Uterine carcinoma is the leading gynecologic malignancy in the United States, for which the number of available therapies is limited. [76] Molecular characterization of endometrial tumors has demonstrated that PIK3CA mutations, PTEN loss, and PI3K and KRAS activation are key events in carcinogenesis. [77,78] In addition to these critical mutations, ErbB2 is amplified in 17-33% of carcinosarcoma, and uterine serous carcinomas. [79,80] Given our findings in ErbB2 mutated or amplified ovarian cancer cell lines, we hypothesized that Grb2 was a critical mediator of oncogenic signaling in uterine carcinomas as well. To assess this, we first performed baseline expression of Grb2 protein expression in a panel of uterine cancer models (**Figure 15A**). We focused on uterine cell line Hec1a known to have erbB2 amplification. Cell viability assay on Hec1a verified sensitivity to Grb2 downregulation compared to control siRNA (**Figure 15B**). Finally we performed RPPA on Hec1a cells transfected with siControl and siGrb2 (**Figure 15C)**. Networks significantly downregulated after siGrb2 transfection include AMPK signaling, PI3K/AKT signaling and Insulin Receptor signaling (**Figure 15D**).

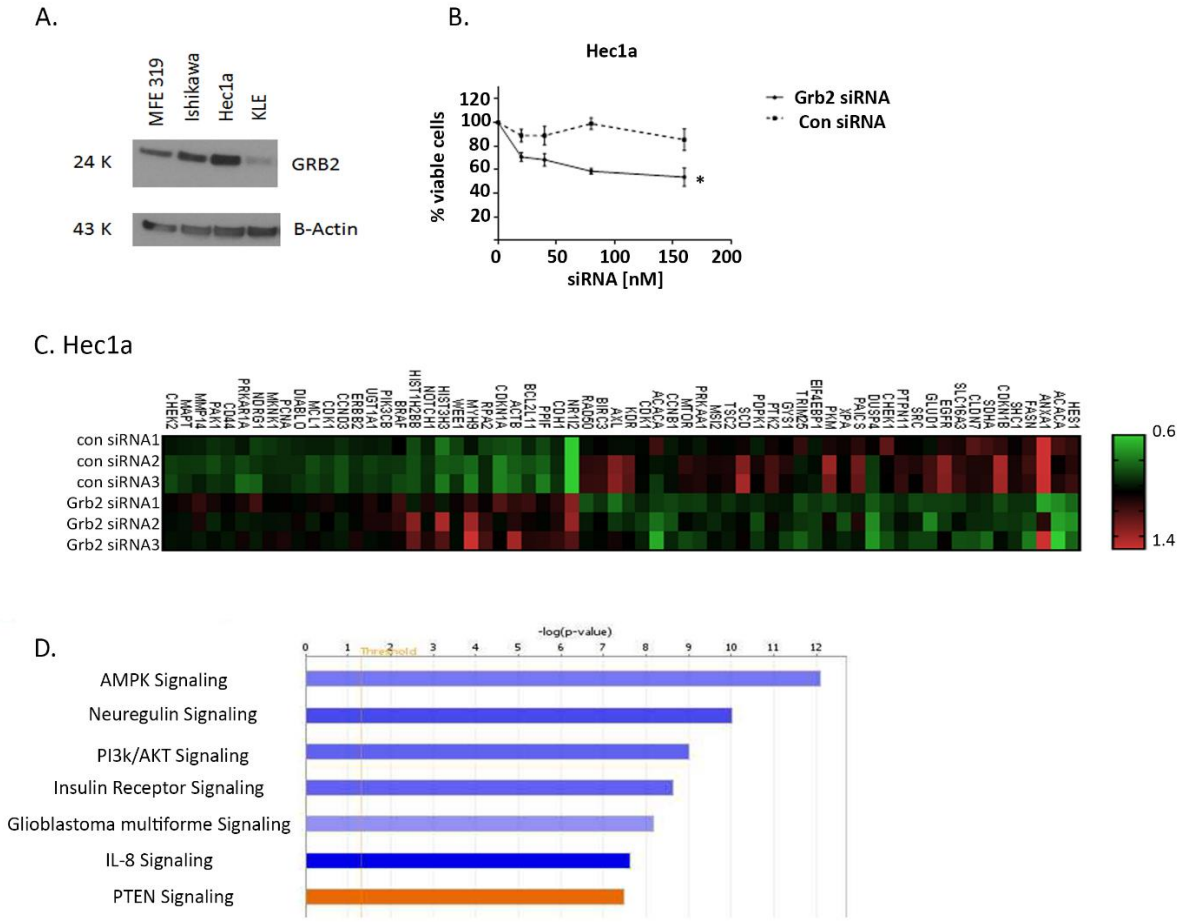

Figure 15. Effect of Grb2 downregulation on uterine cancer cell lines. **A,** Western blot analysis of Grb2 expression in a panel of uterine cancer cell lines. **B,** An alamarBlue assay of Hec1a uterine cancer cells performed 72 hours after transfection to determine their percent viability. Data represent averages of triplicate measurements. **C,** Differential expression of proteins in Hec1A cells after Grb2 downregulation as detected using an RPPA. Heat map of proteins whose expression differed significantly between siGrb2 and siControl transfected groups, p<0.05. **D,** Top canonical pathways generated after Grb2 downregulation using Ingenuity Pathway Analysis (IPA). All statistical tests were two-sided. Asterisk indicates statistical significant of ***p<0.001, **p<0.01, *p<0.05. NS indicates non-significant.

5. Discussion

The key findings form our study include the therapeutic efficacy of L-Grb2 in ovarian preclinical models by increasing cellular apoptosis, and reducing angiogenesis. Additive anti-tumor effects were observed in ovarian tumor models treated with L-Grb2 and paclitaxel. Additionally, L-Grb2 potentiated the effects of anti-angiogenic therapy, B-20, in ovarian models. Finally, we identified cells lines with ErbB2 mutation or overexpression to be particularly sensitive to Grb2 downregulation. This correlated to a decrease in metabolites related to glycolysis and protein synthesis in cell lines after Grb2 inhibition or L-Grb2 treatment.

5.1 Translational Relevance

Targeting Grb2 protein expression through L-Grb2 is a promising molecular therapy of a previously thought to be undruggable target. Given the heterogeneity and large number of molecular alterations in ovarian cancer identifying targets that are of therapeutic benefit is challenging. However, the use of molecular pathways to develop small molecule inhibitors, and personalize individual strategies for treatment remains a promising avenue to improve survival. Grb2 plays a central role in RTK signaling, particularly EGFR and HER2. Approximately 11% of ovarian tumors overexpress HER2, while EGFR overexpression can be as high as 28% and amplified in up to 20% of ovarian cancer patients. [15,81,82] More importantly overexpression of EGFR and ErbB2 has been associated with poor survival prognosis in gynecologic cancer patients.[83] This is likely due to their association with the Ras/Raf/MAPK and PI3K/PTEN/AKT/mTOR pathways, which are activated in 70% and 50% of ovarian cancers, respectively.[15] The high

prevalence of these molecular alterations in ovarian cancer represent an important therapeutic opportunity for L-Grb2.

Given the high rate of reoccurrence and poor prognosis of ovarian cancer, there remains a need for additional lines of therapy that may increase survival but not necessarily be curative. Current targeted and biologic therapies in development or in use in ovarian cancer include antiangiogenic agents, poly (ADP-ribose) polymerase (PARP) inhibitors, immunotherapy, and small molecule inhibitors of signaling pathways. While currently only bevacizumab and PARP inhibitors are FDA-approved as targeted therapy for ovarian cancer patients, the number of small molecule inhibitors in clinical development is growing. As previously mentioned MAPK and PI3K/AKT/mTOR pathways are important cellular signaling pathways involved in proliferation, tumorigenesis, cell survival, angiogenesis, and protein synthesis. Small molecular inhibitors including temsirolimus (TOR complex 1 inhibitor), Pictilisib (PI3K inhibitor), and selumetinib (MEK inhibitor) have had varying efficacy in ovarian cancer patients. These pathways converge at several points, therefore dual blockade or upstream blockade of these pathways may provide synergistic effects and overcome tumor resistance.

The clinical activity of L-Grb2 was recently assessed in a phase 1 trial (BP1001, Bio-Path Holdings) in patients with refractory or relapsed acute myeloid leukemia. Targeting Grb2 is particularly promising in leukemia given the number of activating mutations of tyrosine kinases. BP1001 was well tolerated with anti-leukemic activity as monotherapy and in combination with cytarabine. A maximum tolerated dose was not identified, and the most

common grade 3-4 adverse events were cardiopulmonary disorders (25 [64%] of 39 patients), fever and infections (17 [44%]).[84] Enrollment for a phase 2 study of patients with previously untreated acute myeloid leukemia is underway.

5.2 Study Limitations

Here we show that L-Grb2 has promising activity in preclinical models of ovarian carcinoma. While evidence of L-Grb2 antitumor activity in hematologic malignancies is promising, it is yet to be seen if this can be translated to solid tumors. Additionally therapy targeting erbB2 receptor have had limited success. Another limitation to this work is that only orthotopic ovarian models were investigated, patient derived xenograft models should be considered for future studies.

5.3 Implications and Future Directions

Our preclinical findings support the idea that Grb2 blockade may be an effective treatment for ovarian cancers. Future directions for L-Grb2 include administration as an adjuvant therapy in combination with taxane-based therapy after surgical reduction. Alternatively, L-Grb2 could combine well with bevazicumab, based on our preclinical data. Finally, in patients with high erbB2 expression, lower treatment doses could be considered. Additionally L-Grb2 may prove to be useful in a number of solid malignancies including uterine carcinoma.

In summary, this work introduces a therapy, L-Grb2, which may be beneficial to ovarian cancer patients. Our *in vivo* studies suggest that combination therapy with paclitaxel and anti-angiogenics is well tolerated and provides anti-tumor effects.

Bibliography

1. Siegel RL, Miller KD, Jemal A. Cancer statistics, 2019. *CA Cancer J Clin.* 2019;69(1):7-34.
2. https://seer.cancer.gov/statfacts/html/ovary.html. Accessed 5/9/2019.
3. Prat J. Pathology of cancers of the female genital tract. *Int J Gynaecol Obstet.* 2015;131 Suppl 2:S132-145.
4. Park HK, Ruterbusch JJ, Cote ML. Recent Trends in Ovarian Cancer Incidence and Relative Survival in the United States by Race/Ethnicity and Histologic Subtypes. *Cancer Epidemiol Biomarkers Prev.* 2017;26(10):1511-1518.
5. Kim J, Park EY, Kim O, et al. Cell Origins of High-Grade Serous Ovarian Cancer. *Cancers (Basel).* 2018;10(11).
6. Karnezis AN, Cho KR, Gilks CB, Pearce CL, Huntsman DG. The disparate origins of ovarian cancers: pathogenesis and prevention strategies. *Nat Rev Cancer.* 2017;17(1):65-74.
7. Labidi-Galy SI, Papp E, Hallberg D, et al. High grade serous ovarian carcinomas originate in the fallopian tube. *Nat Commun.* 2017;8(1):1093.
8. Munksgaard PS, Blaakaer J. The association between endometriosis and ovarian cancer: a review of histological, genetic and molecular alterations. *Gynecologic oncology.* 2012;124(1):164-169.
9. Heintz AP, Odicino F, Maisonneuve P, et al. Carcinoma of the ovary. FIGO 26th Annual Report on the Results of Treatment in Gynecological Cancer. *Int J Gynaecol Obstet.* 2006;95 Suppl 1:S161-192.
10. Prat J. FIGO's staging classification for cancer of the ovary, fallopian tube, and peritoneum: abridged republication. *J Gynecol Oncol.* 2015;26(2):87-89.
11. Eisenhauer EA. Real-world evidence in the treatment of ovarian cancer. *Annals of oncology : official journal of the European Society for Medical Oncology.* 2017;28(suppl_8):viii61-viii65.
12. Hudson CN, Chir M. Surgical treatment of ovarian cancer. *Gynecologic oncology.* 1973;1(4):370-378.
13. Chang SJ, Hodeib M, Chang J, Bristow RE. Survival impact of complete cytoreduction to no gross residual disease for advanced-stage ovarian cancer: a meta-analysis. *Gynecologic oncology.* 2013;130(3):493-498.
14. Bristow RE, Tomacruz RS, Armstrong DK, Trimble EL, Montz FJ. Survival effect of maximal cytoreductive surgery for advanced ovarian carcinoma during the platinum era: a meta-analysis. *Journal of clinical oncology : official journal of the American Society of Clinical Oncology.* 2002;20(5):1248-1259.
15. Bast RC, Jr., Hennessy B, Mills GB. The biology of ovarian cancer: new opportunities for translation. *Nat Rev Cancer.* 2009;9(6):415-428.
16. Taylor KN, Eskander RN. PARP Inhibitors in Epithelial Ovarian Cancer. *Recent Pat Anticancer Drug Discov.* 2018;13(2):145-158.
17. Vaughan S, Coward JI, Bast RC, Jr., et al. Rethinking ovarian cancer: recommendations for improving outcomes. *Nat Rev Cancer.* 2011;11(10):719-725.

18. Ahmed AA, Etemadmoghadam D, Temple J, et al. Driver mutations in TP53 are ubiquitous in high grade serous carcinoma of the ovary. *J Pathol.* 2010;221(1):49-56.
19. Integrated genomic analyses of ovarian carcinoma. *Nature.* 2011;474(7353):609-615.
20. Buller RE, Runnebaum IB, Karlan BY, et al. A phase I/II trial of rAd/p53 (SCH 58500) gene replacement in recurrent ovarian cancer. *Cancer Gene Ther.* 2002;9(7):553-566.
21. Mabuchi S, Kuroda H, Takahashi R, Sasano T. The PI3K/AKT/mTOR pathway as a therapeutic target in ovarian cancer. *Gynecologic oncology.* 2015;137(1):173-179.
22. Guan LY, Lu Y. New developments in molecular targeted therapy of ovarian cancer. *Discov Med.* 2018;26(144):219-229.
23. Ho CL, Kurman RJ, Dehari R, Wang TL, Shih Ie M. Mutations of BRAF and KRAS precede the development of ovarian serous borderline tumors. *Cancer Res.* 2004;64(19):6915-6918.
24. Tan DS, Iravani M, McCluggage WG, et al. Genomic analysis reveals the molecular heterogeneity of ovarian clear cell carcinomas. *Clin Cancer Res.* 2011;17(6):1521-1534.
25. Tolcher AW, Peng W, Calvo E. Rational Approaches for Combination Therapy Strategies Targeting the MAP Kinase Pathway in Solid Tumors. *Mol Cancer Ther.* 2018;17(1):3-16.
26. Grisham RN, Iyer G, Garg K, et al. BRAF mutation is associated with early stage disease and improved outcome in patients with low-grade serous ovarian cancer. *Cancer.* 2013;119(3):548-554.
27. Mendivil AA, Tung PK, Bohart R, Bechtol K, Goldstein BH. Dramatic clinical response following dabrafenib and trametinib therapy in a heavily pretreated low grade serous ovarian carcinoma patient with a BRAF V600E mutation. *Gynecol Oncol Rep.* 2018;26:41-44.
28. Martinez-Garcia M, Banerji U, Albanell J, et al. First-in-human, phase I dose-escalation study of the safety, pharmacokinetics, and pharmacodynamics of RO5126766, a first-in-class dual MEK/RAF inhibitor in patients with solid tumors. *Clin Cancer Res.* 2012;18(17):4806-4819.
29. Heist RS, Gandhi L, Shapiro G, et al. Combination of a MEK inhibitor, pimasertib (MSC1936369B), and a PI3K/mTOR inhibitor, SAR245409, in patients with advanced solid tumors: Results of a phase Ib dose-escalation trial. *Journal of Clinical Oncology.* 2013;31(15_suppl):2530-2530.
30. Baselga J, Rischin D, Ranson M, et al. Phase I safety, pharmacokinetic, and pharmacodynamic trial of ZD1839, a selective oral epidermal growth factor receptor tyrosine kinase inhibitor, in patients with five selected solid tumor types. *Journal of clinical oncology : official journal of the American Society of Clinical Oncology.* 2002;20(21):4292-4302.
31. Vasey PA, Jayson GC, Gordon A, et al. Phase III randomized trial of docetaxel-carboplatin versus paclitaxel-carboplatin as first-line chemotherapy for ovarian carcinoma. *J Natl Cancer Inst.* 2004;96(22):1682-1691.

32. Bookman MA, Darcy KM, Clarke-Pearson D, Boothby RA, Horowitz IR. Evaluation of monoclonal humanized anti-HER2 antibody, trastuzumab, in patients with recurrent or refractory ovarian or primary peritoneal carcinoma with overexpression of HER2: a phase II trial of the Gynecologic Oncology Group. *Journal of clinical oncology : official journal of the American Society of Clinical Oncology.* 2003;21(2):283-290.
33. Lemmon MA, Schlessinger J. Cell signaling by receptor tyrosine kinases. *Cell.* 2010;141(7):1117-1134.
34. Pawson T, Scott JD. Signaling through scaffold, anchoring, and adaptor proteins. *Science (New York, N.Y.).* 1997;278(5346):2075-2080.
35. Luo LY, Hahn WC. Oncogenic Signaling Adaptor Proteins. *J Genet Genomics.* 2015;42(10):521-529.
36. Buday L, Downward J. Epidermal growth factor regulates p21ras through the formation of a complex of receptor, Grb2 adapter protein, and Sos nucleotide exchange factor. *Cell.* 1993;73(3):611-620.
37. Egan SE, Giddings BW, Brooks MW, Buday L, Sizeland AM, Weinberg RA. Association of Sos Ras exchange protein with Grb2 is implicated in tyrosine kinase signal transduction and transformation. *Nature.* 1993;363(6424):45-51.
38. Chardin P, Camonis JH, Gale NW, et al. Human Sos1: a guanine nucleotide exchange factor for Ras that binds to GRB2. *Science (New York, N.Y.).* 1993;260(5112):1338-1343.
39. Gale NW, Kaplan S, Lowenstein EJ, Schlessinger J, Bar-Sagi D. Grb2 mediates the EGF-dependent activation of guanine nucleotide exchange on Ras. *Nature.* 1993;363(6424):88-92.
40. Wang J, Auger KR, Jarvis L, Shi Y, Roberts TM. Direct association of Grb2 with the p85 subunit of phosphatidylinositol 3-kinase. *J Biol Chem.* 1995;270(21):12774-12780.
41. Lowenstein EJ, Daly RJ, Batzer AG, et al. The SH2 and SH3 domain-containing protein GRB2 links receptor tyrosine kinases to ras signaling. *Cell.* 1992;70(3):431-442.
42. Rask-Andersen M, Masuram S, Schioth HB. The druggable genome: Evaluation of drug targets in clinical trials suggests major shifts in molecular class and indication. *Annu Rev Pharmacol Toxicol.* 2014;54:9-26.
43. Bunnage ME, Chekler EL, Jones LH. Target validation using chemical probes. *Nat Chem Biol.* 2013;9(4):195-199.
44. Wang WT, Han C, Sun YM, Chen TQ, Chen YQ. Noncoding RNAs in cancer therapy resistance and targeted drug development. *J Hematol Oncol.* 2019;12(1):55.
45. Barata P, Sood AK, Hong DS. RNA-targeted therapeutics in cancer clinical trials: Current status and future directions. *Cancer Treat Rev.* 2016;50:35-47.
46. Fire A, Xu S, Montgomery MK, Kostas SA, Driver SE, Mello CC. Potent and specific genetic interference by double-stranded RNA in Caenorhabditis elegans. *Nature.* 1998;391(6669):806-811.
47. Agrawal N, Dasaradhi PV, Mohmmed A, Malhotra P, Bhatnagar RK, Mukherjee SK. RNA interference: biology, mechanism, and applications. *Microbiol Mol Biol Rev.* 2003;67(4):657-685.

48. Lam JKW, Chow MYT, Zhang Y, Leung SWS. siRNA Versus miRNA as Therapeutics for Gene Silencing. *Molecular Therapy - Nucleic Acids.* 2015;4:e252.
49. Ha M, Kim VN. Regulation of microRNA biogenesis. *Nature Reviews Molecular Cell Biology.* 2014;15:509.
50. Hemmings-Mieszczak M, Dorn G, Natt FJ, Hall J, Wishart WL. Independent combinatorial effect of antisense oligonucleotides and RNAi-mediated specific inhibition of the recombinant rat P2X3 receptor. *Nucleic Acids Res.* 2003;31(8):2117-2126.
51. McCaffrey AP, Meuse L, Pham TT, Conklin DS, Hannon GJ, Kay MA. RNA interference in adult mice. *Nature.* 2002;418(6893):38-39.
52. Sercombe L, Veerati T, Moheimani F, Wu SY, Sood AK, Hua S. Advances and Challenges of Liposome Assisted Drug Delivery. *Front Pharmacol.* 2015;6:286.
53. Kaczmarek JC, Kowalski PS, Anderson DG. Advances in the delivery of RNA therapeutics: from concept to clinical reality. *Genome medicine.* 2017;9(1):60-60.
54. Campbell PI. Toxicity of some charged lipids used in liposome preparations. *Cytobios.* 1983;37(145):21-26.
55. Nakanishi T, Kunisawa J, Hayashi A, et al. Positively charged liposome functions as an efficient immunoadjuvant in inducing cell-mediated immune response to soluble proteins. *J Control Release.* 1999;61(1-2):233-240.
56. Xia Y, Tian J, Chen X. Effect of surface properties on liposomal siRNA delivery. *Biomaterials.* 2016;79:56-68.
57. Senior JH, Trimble KR, Maskiewicz R. Interaction of positively-charged liposomes with blood: implications for their application *in vivo*. *Biochim Biophys Acta.* 1991;1070(1):173-179.
58. Zhao W, Zhuang S, Qi XR. Comparative study of the *in vitro* and *in vivo* characteristics of cationic and neutral liposomes. *Int J Nanomedicine.* 2011;6:3087-3098.
59. Dutta P, Perez MR, Lee J, et al. Combining hyperpolarized real-time metabolic imaging and NMR spectroscopy to identify metabolic biomarkers in pancreatic cancer. *Journal of proteome research.* 2019.
60. Zacharias NM, McCullough C, Shanmugavelandy S, et al. Metabolic Differences in Glutamine Utilization Lead to Metabolic Vulnerabilities in Prostate Cancer. *Sci Rep.* 2017;7(1):16159.
61. Pounds S, Morris SW. Estimating the occurrence of false positives and false negatives in microarray studies by approximating and partitioning the empirical distribution of p-values. *Bioinformatics (Oxford, England).* 2003;19(10):1236-1242.
62. Domcke S, Sinha R, Levine DA, Sander C, Schultz N. Evaluating cell lines as tumour models by comparison of genomic profiles. *Nature Communications.* 2013;4:2126.
63. Previs RA, Armaiz-Pena GN, Ivan C, et al. Role of YAP1 as a Marker of Sensitivity to Dual AKT and P70S6K Inhibition in Ovarian and Uterine Malignancies. *J Natl Cancer Inst.* 2017;109(7).
64. Warburg O. On respiratory impairment in cancer cells. *Science (New York, N.Y.).* 1956;124(3215):269-270.

65. Kroemer G, Pouyssegur J. Tumor cell metabolism: cancer's Achilles' heel. *Cancer cell.* 2008;13(6):472-482.
66. Vander Heiden MG, Cantley LC, Thompson CB. Understanding the Warburg effect: the metabolic requirements of cell proliferation. *Science (New York, N.Y.).* 2009;324(5930):1029-1033.
67. Stine ZE, Walton ZE, Altman BJ, Hsieh AL, Dang CV. MYC, Metabolism, and Cancer. *Cancer Discov.* 2015;5(10):1024-1039.
68. Gordan JD, Thompson CB, Simon MC. HIF and c-Myc: sibling rivals for control of cancer cell metabolism and proliferation. *Cancer cell.* 2007;12(2):108-113.
69. Goetzman ES, Prochownik EV. The Role for Myc in Coordinating Glycolysis, Oxidative Phosphorylation, Glutaminolysis, and Fatty Acid Metabolism in Normal and Neoplastic Tissues. *Front Endocrinol (Lausanne).* 2018;9:129-129.
70. Rajeshkumar NV, Dutta P, Yabuuchi S, et al. Therapeutic Targeting of the Warburg Effect in Pancreatic Cancer Relies on an Absence of p53 Function. *Cancer Research.* 2015;75(16):3355-3364.
71. Fu Y, Liu S, Yin S, et al. The reverse Warburg effect is likely to be an Achilles' heel of cancer that can be exploited for cancer therapy. *Oncotarget.* 2017;8(34):57813-57825.
72. Kaczanowski S, Klim J, Zielenkiewicz U. An Apoptotic and Endosymbiotic Explanation of the Warburg and the Inverse Warburg Hypotheses. *Int J Mol Sci.* 2018;19(10):3100.
73. Sia D, Alsinet C, Newell P, Villanueva A. VEGF signaling in cancer treatment. *Current pharmaceutical design.* 2014;20(17):2834-2842.
74. Simons M, Gordon E, Claesson-Welsh L. Mechanisms and regulation of endothelial VEGF receptor signalling. *Nature Reviews Molecular Cell Biology.* 2016;17:611.
75. Ferrara N, Gerber HP, LeCouter J. The biology of VEGF and its receptors. *Nature medicine.* 2003;9(6):669-676.
76. Diver EJ, Foster R, Rueda BR, Growdon WB. The Therapeutic Challenge of Targeting HER2 in Endometrial Cancer. *Oncologist.* 2015;20(9):1058-1068.
77. Berg A, Hoivik EA, Mjøs S, et al. Molecular profiling of endometrial carcinoma precursor, primary and metastatic lesions suggests different targets for treatment in obese compared to non-obese patients. *Oncotarget.* 2014;6(2):1327-1339.
78. Bradford LS, Rauh-Hain A, Clark RM, et al. Assessing the efficacy of targeting the phosphatidylinositol 3-kinase/AKT/mTOR signaling pathway in endometrial cancer. *Gynecologic oncology.* 2014;133(2):346-352.
79. Slomovitz BM, Broaddus RR, Burke TW, et al. Her-2/neu overexpression and amplification in uterine papillary serous carcinoma. *Journal of clinical oncology : official journal of the American Society of Clinical Oncology.* 2004;22(15):3126-3132.
80. Santin AD, Bellone S, Van Stedum S, et al. Amplification of c-erbB2 oncogene: a major prognostic indicator in uterine serous papillary carcinoma. *Cancer.* 2005;104(7):1391-1397.
81. Reibenwein J, Krainer M. Targeting signaling pathways in ovarian cancer. *Expert Opin Ther Targets.* 2008;12(3):353-365.

82. Zanini E, Louis LS, Antony J, et al. The Tumor-Suppressor Protein OPCML Potentiates Anti-EGFR- and Anti-HER2-Targeted Therapy in HER2-Positive Ovarian and Breast Cancer. *Mol Cancer Ther.* 2017;16(10):2246-2256.
83. Luo H, Xu X, Ye M, Sheng B, Zhu X. The prognostic value of HER2 in ovarian cancer: A meta-analysis of observational studies. *PLoS One.* 2018;13(1):e0191972.
84. Ohanian M, Tari Ashizawa A, Garcia-Manero G, et al. Liposomal Grb2 antisense oligodeoxynucleotide (BP1001) in patients with refractory or relapsed haematological malignancies: a single-centre, open-label, dose-escalation, phase 1/1b trial. *Lancet Haematol.* 2018;5(4):e136-e146.

Vita

Olivia was born in Uvalde, Texas, the daughter of Robert and Martha Lara. After completing her work at Uvalde High School she entered Texas A&M University in College Station, Texas. She received the degree of Bachelor of Arts with a major in chemistry May, 2008. She attended the University of Texas Health Science Center at San Antonio, San Antonio, Texas and graduated with a Doctor of Medicine in 2013. She entered the Obstetrics and Gynecologic residency program at Dell Medical School, Austin, Texas, completing her training in 2017. In July 2017, she began a post-doctoral research fellowship in Surgical Oncology at the University of Texas M.D. Anderson Cancer Center. Her two year Master's program during this fellowship was mentored by Dr. Anil K. Sood and focused on the development of novel therapeutics in ovarian and uterine malignancies including L-Grb2 (BP1001).

Permanent Address:

3121 Buffalo Speedway, Apt 2109

Houston, TX 77098